iScience

CellPress
OPEN ACCESS

Article

Glioblastoma Utilizes Fatty Acids and Ketone Bodies for Growth Allowing Progression during Ketogenic Diet Therapy

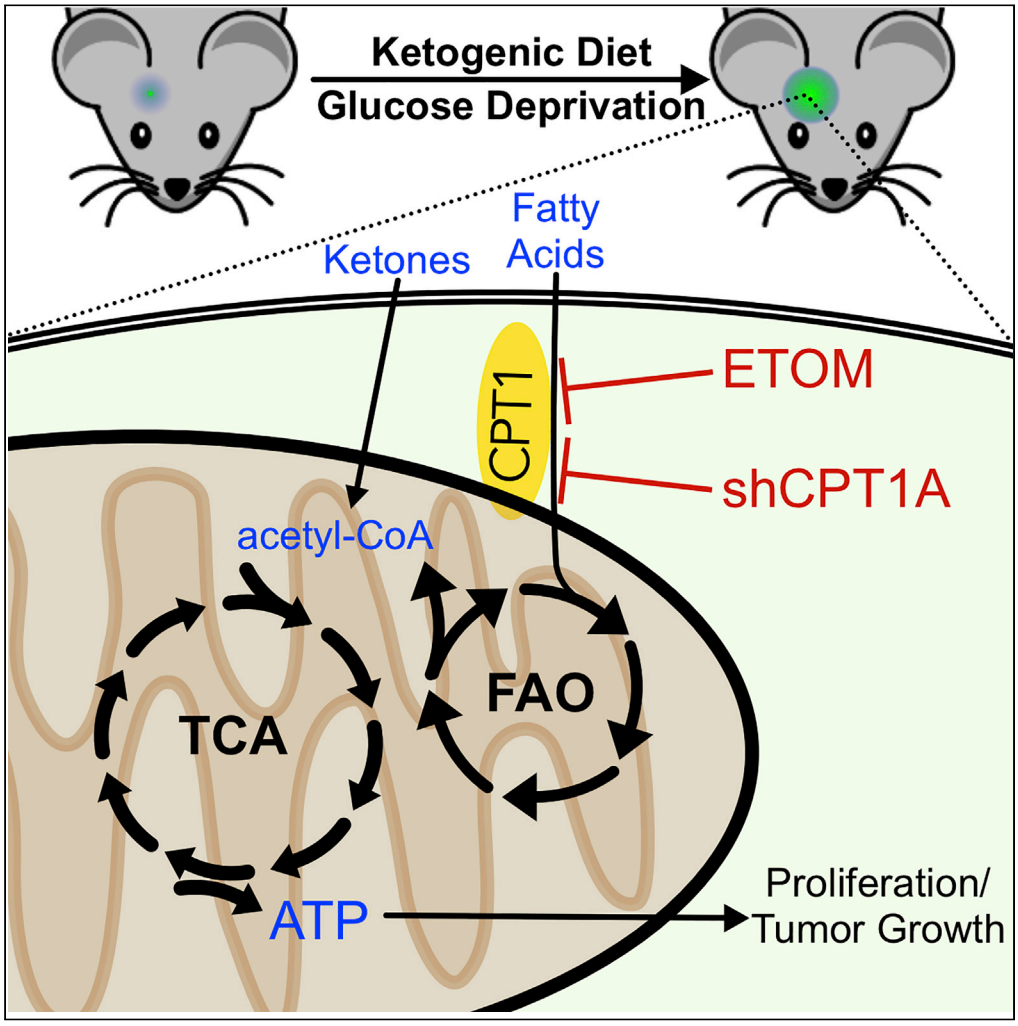

Jantzen Sperry, Michael C. Condro, Lea Guo, ..., Pedro R. Lowenstein, Janel E. Le Belle, Harley I. Kornblum

hkornblum@mednet.ucla.edu

HIGHLIGHTS

Glioblastoma cells can use fatty acid oxidation and ketones for energy requirements

Inhibition of fatty acid oxidation reduces glioblastoma growth *in vivo* and *in vitro*

Unrestricted ketogenic diet does not reduce tumor growth in multiple models of GBM

IDH1 mutant glioblastomas may use FAO differently than IDH wild-type tumors

Sperry et al., iScience *23*, 101453
September 25, 2020
https://doi.org/10.1016/j.isci.2020.101453

iScience

CellPress
OPEN ACCESS

Article

Glioblastoma Utilizes Fatty Acids and Ketone Bodies for Growth Allowing Progression during Ketogenic Diet Therapy

Jantzen Sperry,[1,10] Michael C. Condro,[2] Lea Guo,[2,3] Daniel Braas,[4] Nathan Vanderveer-Harris,[2] Kristen K.O. Kim,[1] Whitney B. Pope,[3] Ajit S. Divakaruni,[1] Albert Lai,[5,6] Heather Christofk,[1,5,7,8] Maria G. Castro,[9] Pedro R. Lowenstein,[9] Janel E. Le Belle,[2] and Harley I. Kornblum[1,2,5,8,11,*]

SUMMARY

Glioblastoma (GBM) metabolism has traditionally been characterized by a primary dependence on aerobic glycolysis, prompting the use of the ketogenic diet (KD) as a potential therapy. In this study we evaluated the effectiveness of the KD in GBM and assessed the role of fatty acid oxidation (FAO) in promoting GBM propagation. *In vitro* assays revealed FA utilization throughout the GBM metabolome and growth inhibition in nearly every cell line in a broad spectrum of patient-derived glioma cells treated with FAO inhibitors. *In vivo* assessments revealed that knockdown of carnitine palmitoyltransferase 1A (CPT1A), the rate-limiting enzyme for FAO, reduced the rate of tumor growth and increased survival. However, the unrestricted ketogenic diet did not reduce tumor growth and for some models significantly reduced survival. Altogether, these data highlight important roles for FA and ketone body metabolism that could serve to improve targeted therapies in GBM.

INTRODUCTION

Normally, the adult brain meets most of its energy demand by complete oxidation of glucose, producing pyruvate, which is converted into acetyl-CoA for entrance into the TCA cycle to support the electron transport chain (Agnihotri and Zadeh, 2016). Thus, glycolysis and respiration remain tightly linked, resulting in efficient ATP production with little lactic acid production. On the other hand, many tumors, including the universally lethal glioblastoma (GBM), utilize the Warburg effect (Vander Heiden et al., 2009), which dramatically increases the rate of aerobic glycolysis and lactate production in the cytosol. This process allows for increased biomass production and facilitated invasion through acidification of the microenvironment among other things.

The signaling pathways hyperactivated in GBM and the underlying mutations significantly influence GBM metabolism. Numerous oncogenic mutations activate the PI3K/AKT/mTOR signaling pathway, which promotes glucose utilization and the Warburg effect (Yang et al., 2019). The net result of these mutations is to both utilize glucose as an energy substrate and to promote FA synthesis for membrane biogenesis (Furuta et al., 2008). Thus, GBM-causing mutations induce what has been called a "glucose addiction," which one might target directly by limiting glucose availability. The effects of some other mutations, such as those in the isocitrate dehydrogenase (IDH) 1 and 2 genes on glucose utilization and dependence, are less clear.

Brain neurons utilize glucose as a primary energy source under normal physiological conditions, and upon glucose deprivation neurons readily utilize ketone bodies (KBs) as an alternative fuel (Maurer et al., 2011). Glial cells are also capable of using KBs and FAs for fuel (Lopes-Cardozo et al., 1986; Weightman Potter et al., 2019). Thus, one might reason that treatments that inhibit glucose metabolism and promote FA and KB metabolism would be ideal for treating tumors that are known to be glucose addicted. Indeed, the ketogenic diet (KD), which consists of high fat, low carbohydrates, and adequate protein, has long been used in the treatment of epilepsy and has recently been proposed as a potential adjuvant therapy for a number of cancers including GBM (Maurer et al., 2011; Vidali et al., 2015). In some animal studies, the KD has indeed shown preliminary efficacy (Abdelwahab et al., 2012; Mukherjee et al., 2019), and a number of glioma patients have initiated KD therapy.

[1]Department of Molecular and Medical Pharmacology, David Geffen School of Medicine, University of California, Los Angeles, CA 90095, USA

[2]Department of Psychiatry and Biobehavioral Sciences and Semel Institute for Neuroscience & Human Behavior, UCLA, Los Angeles, CA, USA

[3]Department of Radiological Sciences, David Geffen School of Medicine, UCLA, Los Angeles, CA, USA

[4]UCLA Metabolomics Center, UCLA, Los Angeles, CA, USA

[5]Jonsson Comprehensive Cancer Center, UCLA, Los Angeles, CA, USA

[6]Department of Neurology, UCLA, Los Angeles, CA, USA

[7]Department of Biological Chemistry, UCLA, Los Angeles, CA, USA

[8]Eli and Edythe Broad Center of Regenerative Medicine and Stem Cell Research, UCLA, Los Angeles, CA, USA

[9]Department of Neurosurgery, Department of Cell and Developmental Biology, Rogel Cancer Center, University of Michigan Medical School, Ann Arbor, MI 48109, USA

[10]Present address: Certis Oncology Solutions, San Diego, CA 92121, USA

[11]Lead Contact

*Correspondence: hkornblum@mednet.ucla.edu

https://doi.org/10.1016/j.isci.2020.101453

Despite the potential for utilizing the KD as a therapy for glioma, there are factors that may mitigate enthusiasm. First, not all animal studies using the KD have demonstrated efficacy (De Feyter et al., 2016). Another factor to consider is glioma heterogeneity. In addition to there being multiple molecular subtypes of GBM (Lee et al., 2018), with some mutations that may not create glucose addiction, there is a high degree of intratumoral heterogeneity. In some regions of GBM there is relative hypoxia that could alter the tumor's ability to utilize glucose via the Warburg effect (Kim et al., 2006). These properties may be exacerbated by therapies that limit vascular supply, selecting for those cells most capable of surviving under harsh conditions. Recent studies have indicated that GBMs could be utilizing FAs as both energy sources and as substrates for generating cellular building blocks (Strickland and Stoll, 2017). However, it is unknown whether FAO occurs across the mutational spectrum of GBM. Nor has it been demonstrated precisely how FAs are utilized or whether the KD itself may supply FAs and/or KBs.

Here we demonstrate that the well-characterized U87 glioma cell line and patient-derived GBM cultures, including those with mutations in the PI3K/AKT/mTOR pathways and the IDH1 gene, utilize FAs and KBs for growth under physiologic and standard cell culture conditions. Metabolic tracing studies indicate FAs are oxidized and incorporated into TCA cycle intermediates. Furthermore, administration of the non-calorie-restricted KD to tumor-bearing animals does not decrease the rate of tumor growth, nor does it improve animal survival. Knockdown of CPT1A, the rate-limiting enzyme for FAO, or its inhibition by etomoxir alters the metabolic profile and growth of GBM *in vitro*. These data highlight the metabolic plasticity of GBM and caution against universal use of the KD as adjuvant therapy, although they do not preclude combining the KD with other metabolic therapies and do not address the potential for calorie-restricted KD utilization.

RESULTS

Fatty Acid and Ketone Oxidation in Glioma Cells

In order to determine whether GBMs are capable of oxidizing fatty acids we first examined expression levels of *CPT1*, the rate-limiting enzyme required for FAO, in U87 cells. Although the precise origin of this cell line is not known, a recent study has validated it as a bona fide glioblastoma line (Allen et al., 2016), and it is widely used as a model in glioma research, especially in metabolic studies including studies of fatty acid metabolism (Guo et al., 2009). Analysis of the TCGA dataset from GBM tumors reveals that of the three *CPT1* isoforms found in humans, *CPT1A* and *CPT1C* are most highly expressed in GBM and that *CPT1B* is expressed at lower levels (Figure 1A). Because the TCGA data are derived from whole tumors, we utilized a single cell RNA seq dataset (Darmanis et al., 2017) to verify the expression of CPT isoforms, as well as the major enzymes involved in fatty acid beta oxidation, within tumor cells themselves, and that the levels of expression of these genes were comparable to those of fatty acid synthesis (Figure S1).

To assess a potential role for FAO in gliomas, we treated U87 GBM cells with the CPT1-specific inhibitor etomoxir (ETOM) *in vitro* and found that it modestly inhibited growth under standard, serum-free conditions (Figure 1B). In addition, shRNA-mediated partial (68%) knockdown of CPT1A alone was sufficient to significantly inhibit *in vitro* cell growth by ~40% to levels near those observed with ETOM alone (Figure 1B), suggesting that the CPT1A isoform predominantly contributes to FAO in these cells. Importantly, this demonstrates that endogenous FAO contributes to the maintenance of normal *in vitro* cell growth in these GBM cells despite U87s having a PTEN mutation with increased PI3K/AKT/mTOR signaling, which has been previously thought to inhibit FAO in GBM. Because gliomasphere media used for *in vitro* studies contains levels of glucose (25 mM) not likely to be found naturally in the human brain or in brain tumors, a glucose-limiting assay was performed to assess both fatty acid and ketone body utilization under more physiologically relevant glucose levels, with 2.5 mM glucose representing extracellular levels commonly found in the brain and 1 mM glucose serving as a low glucose condition to more closely mimic levels found in tissue that do not have adequate access to vascular supplies of glucose (Silver and Erecińska, 1994). Palmitic acid supplementation (50–100 μM) increased U87 cell growth under 2.5 mM low glucose conditions (Figure 1C), whereas ketone supplementation with 2.5–5 mM 3-hydroxybutyrate (3-OHB) promoted cell growth in both 2.5 mM and 1 mM glucose (Figure 1D). Higher levels of supplementation (200 μM palmitic acid and 10 mM 3-OHB) resulted in a reversal of the proliferative effects, likely due to toxicity of these supplements at higher concentrations, as has been described for neural stem cells and another tumor cell line (Park et al., 2011; Poff et al., 2014). Neither FA nor ketone supplementation had growth-promoting effects under non-physiological conditions of high glucose (25 mM).

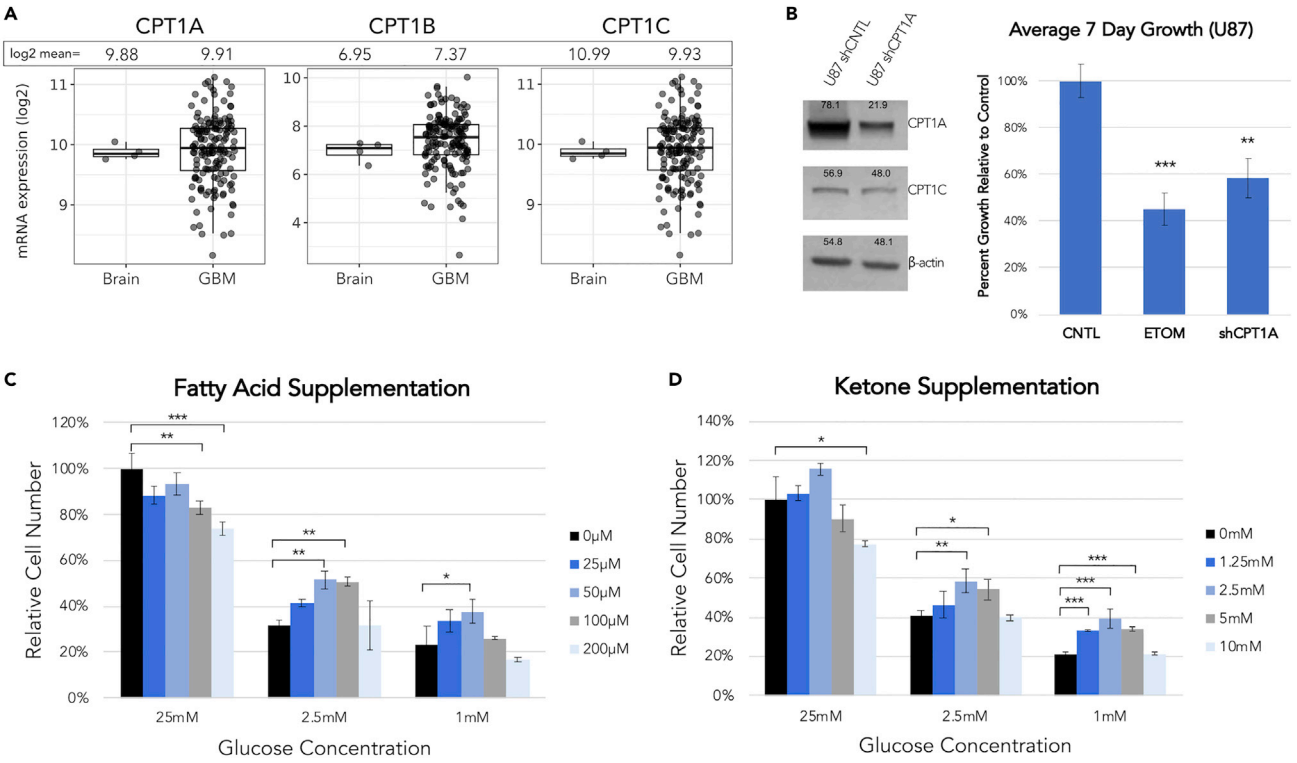

Figure 1. U87 GBM Cells Oxidize Fatty Acids and Ketone Bodies to Support Growth

(A) Relative mRNA expression of the three CPT1 isoforms in GBM based on analysis of the TCGA dataset from patient-derived GBM tumors. N = 4 non-tumor, N = 156 GBM. See also Figure S1.

(B) Quantification of the effects of 100 mM ETOM treatment and shRNA targeting CPT1A on U87 cell growth. Culture growth was assessed following a 7 day treatment with ETOM administered twice per week. n = 3 replicates. Error bars indicate ± SD. Univariate generalized linear model $F(2,5) = 47.37$, $p = 5.6x10^{-4}$, post-hoc Tukey HSD (** = $p<0.01$; *** = $p<0.001$).

(C and D). Effects of FA (C) and ketone (D) supplementation under variable concentrations of glucose following a 7 day growth period in U87 cells. n = 3 replicates. For all univariate generalized linear models for different concentrations of supplements within each glucose concentration $p<0.01$. Post-hoc Tukey HSD significance is reported for each supplement concentration against its control. Error bars denote ± SD. (* = $p<0.05$; ** = $p<0.01$; *** = $p<0.001$).

To further determine how and where FAs are utilized within U87 cells, untreated CNTL cells, cells treated with ETOM, and cells with CPT1A knockdown were subjected to LC-MS metabolomic analysis using fully labeled ^{13}C palmitic acid in physiological glucose conditions (2.5 mM). Analyzing fractional contribution (i.e. the percent contribution of carbons in each metabolite from radiolabeled palmitate) within these samples revealed labeling throughout the TCA cycle as well as in the ubiquitously important currency metabolite ATP, indicating that FAO contributed to the pool of carbons used in the synthesis of these metabolites. Treatment with ETOM- or CRISPR-based CPT1A knockdown (Figure S2) dramatically diminished this labeling (Figure 2A). Similar effects were observed when analyzing the relative amounts of these metabolites, wherein ETOM treatment and CPT1A knockdown significantly decrease levels of TCA-associated metabolites, acetyl-CoA, and ATP (Figure 2B). The effects of FAO inhibition on relative amounts of metabolites demonstrates that inhibiting FAO affects production of these metabolites via unclear mechanisms, as the oxidation of even chain fatty acids should not make a net contribution to carbons in intermediary metabolites. Taken together, these data confirm that GBM cells actively oxidize FAs and suggest that of the three CPT1 isoforms, CPT1A appears to be the primary isoform regulating this process in the U87 line.

CPT1A Knockdown and the Ketogenic Diet

Based on these initial results and previous studies (Seyfried et al., 2003; Skinner et al., 2009) that have indicated that many brain tumors may lack the ability to oxidize ketones as an energy substrate, we sought to determine if inhibiting FAO while concurrently implementing a KD using an orthotopic xenograft model in mice might serve as an effective therapeutic strategy. It is thought that this strategy would reduce the availability of glucose as an energy substrate and make the GBM cells more vulnerable to cell death (starvation)

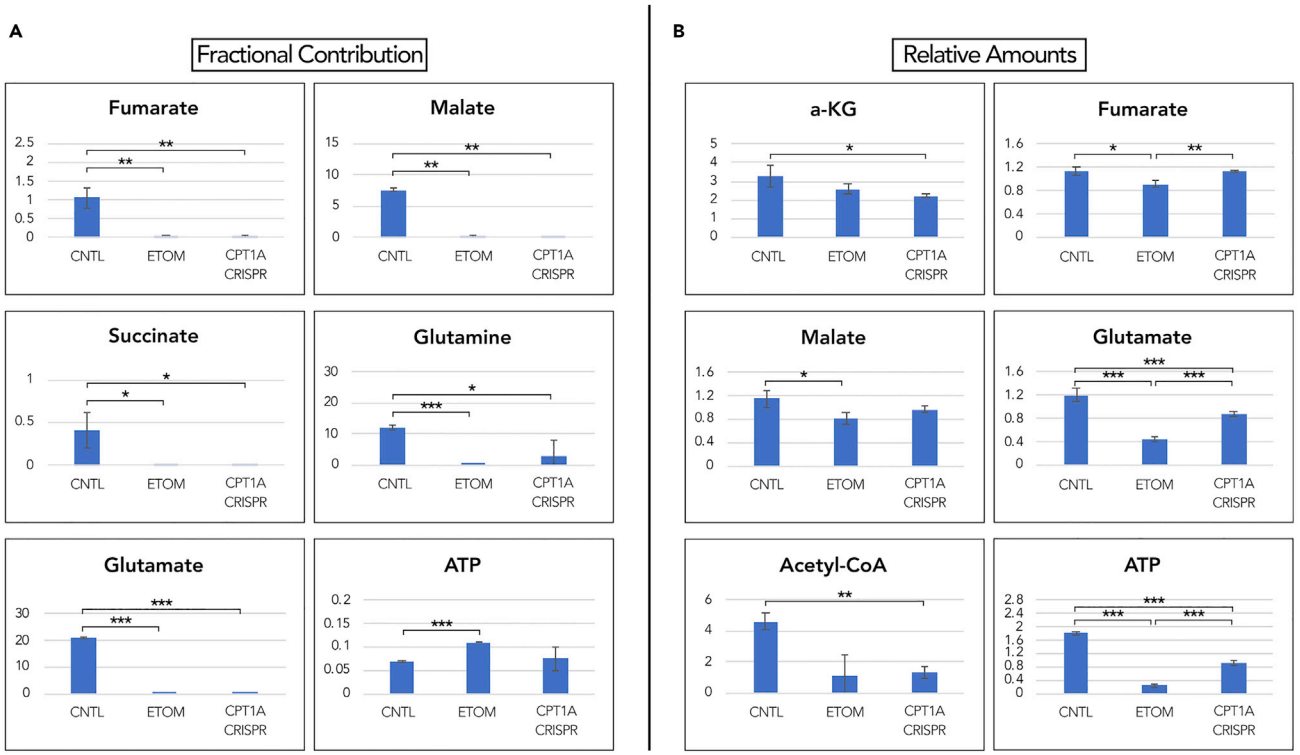

Figure 2. U87 GBM Cells Oxidize Fatty Acids to Generate TCA Cycle Intermediates and Currency Metabolites

(A and B) Effects of ETOM and CPT1A knockdown in U87 cells on fractional contribution (the percent contribution of carbons from radiolabeled palmitate) and relative amounts of relevant TCA cycle intermediates and currency metabolites using ^{13}C-palmitate LC-MS analysis. Glucose concentration = 2.5 mM. n = 3 replicates. Error bars = ± SD (* = $p < 0.05$, ** = $p < 0.01$, *** = $p < 0.001$).

See also Figure S2.

by also inhibiting FAO as an alternative energy source. To assess these results *in vivo*, as well as to determine the effectiveness of the KD on tumor growth, U87 cells expressing a firefly luciferase-GFP reporter (FLuc-GFP) and either shCNTL or shCPT1A were implanted unilaterally into the striatum of adult NSG mice. Four days after implantation, half of each group was switched to a calorie-unrestricted KD followed by weekly bioluminescent imaging with luciferin (Figure 3A). At 21 days post-injection, animal weights, blood glucose levels, and blood ketone levels were evaluated. Both of the KD cohorts (shCNTL and shCPT1A) exhibited decreased total body weight, decreased blood glucose levels, and increased blood 3-OHB levels, confirming ketosis was achieved in these animals (Figure 3B). Contrary to our initial hypothesis, analysis from weekly bioluminescent imaging shows that the shCNTL cohort receiving the KD had the greatest increase in tumor size, although the difference between this group and the shCNTL standard diet (STD) group was not significant (Figure 3C). Survival analysis also indicated that this group had the poorest survival (Figure 3D), supporting the hypothesis that the KD contributed to tumor growth in this cohort. Importantly the growth of the tumors treated with the KD was significantly diminished (Figure 3C) and survival enhanced (Figure 3D) by CPT1A knockdown. CPT1A knockdown resulted in a decrease in tumor growth and enhanced survival in the mice on the standard diet as well, suggesting that FAO contributes to tumor growth even under normal dietary conditions. Immunohistochemistry of sectioned postmortem tissue confirmed that CPT1A knockdown was maintained throughout the length of the experiment (Figure 3E). The findings using our model, although surprising, may indicate that at the very least ketosis does not hinder GBM growth and may exacerbate it in some tumors, while also highlighting an important role of CPT1A-mediated FAO in tumor growth in general.

Patient-Derived GBM Gliomasphere Cultures

To further assess inhibition of endogenous FAO on GBM cell growth and survival we tested the effects of ETOM in a panel of patient-derived GBM cultures. These experiments were done under high glucose conditions with the minimal exogenous fatty acids present in B27 supplement. A seven-day treatment with

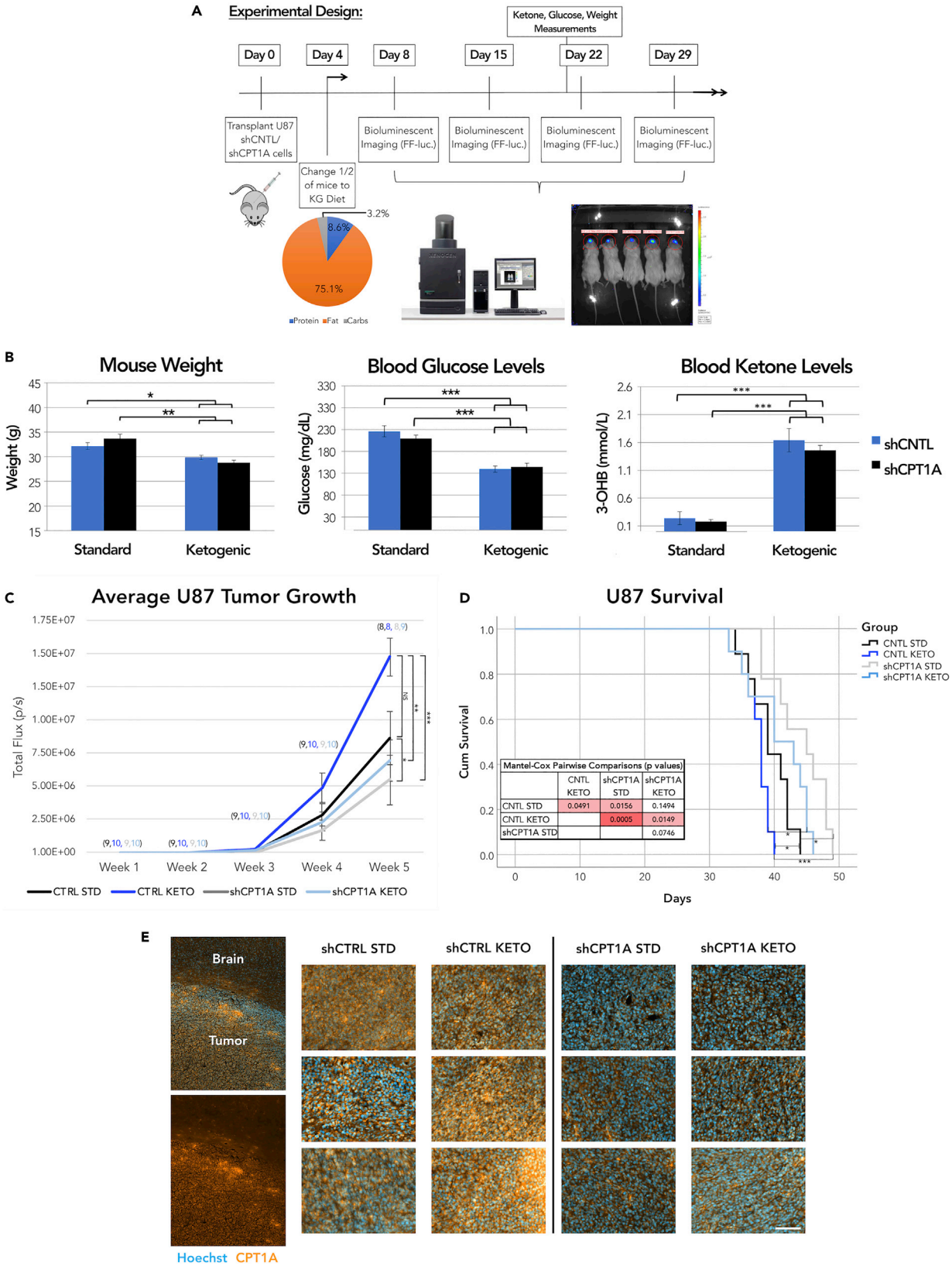
A
Experimental Design:
Ketone, Glucose, Weight Measurements
Day 0
Day 4
Day 8
Day 15
Day 22
Day 29
Transplant U87 shCNTL/ shCPT1A cells
Change 1/2 of mice to KG Diet
Bioluminescent Imaging (FF-luc.)
Bioluminescent Imaging (FF-luc.)
Bioluminescent Imaging (FF-luc.)
Bioluminescent Imaging (FF-luc.)
3.2%
8.6%
75.1%
Protein Fat Carbs
B
Mouse Weight
Weight (g)
Standard
Ketogenic
Blood Glucose Levels
Glucose (mg/dL)
Blood Ketone Levels
3-OHB (mmol/L)
shCNTL
shCPT1A
C
Average U87 Tumor Growth
Total Flux (p/s)
Week 1
Week 2
Week 3
Week 4
Week 5
CTRL STD
CTRL KETO
shCPT1A STD
shCPT1A KETO
D
U87 Survival
Cum Survival
Days
Group
CNTL STD
CNTL KETO
shCPT1A STD
shCPT1A KETO
Mantel-Cox Pairwise Comparisons (p values)
CNTL KETO
shCPT1A STD
shCPT1A KETO
CNTL STD 0.0491 0.0156 0.1494
CNTL KETO 0.0005 0.0149
shCPT1A STD 0.0746
E
Brain
Tumor
Hoechst CPT1A
shCTRL STD
shCTRL KETO
shCPT1A STD
shCPT1A KETO

Figure 3. Knockdown of CPT1A, but Not Ketogenic Diet, Decreases U87 Tumor Growth *In Vivo*

(A) Basic schematic of the experimental design for the U87 shCPT1A ketogenic diet xenotransplant experiment. Cells were implanted into 10 mice per group on Day 0. Mice were kept on standard diet for 4 days to allow appropriate recovery, after which half of each group was placed on the ketogenic diet. Weekly bioluminescent imaging was initiated on Day 8.

(B) On Day 21 mouse weight, blood glucose and ketones were measured. Error bars denote ±SEM. Mixed effects model $F(3,55.111) = 4.401$, $p = 0.0076$. Last time point $F(3,29) = 5.618$, $p = 0.0037$, pairwise comparison significance values are noted in the figure.

(C) Average tumor growth based on total flux (photons/s) from the firefly luciferase (Error bars = ± SEM). Numbers in parentheses indicate the number of animals measured at each time point. Mixed effects model with repeated measures $F(1,4,3) = 4.401$, $p = 0.008$, followed by pairwise post-hoc Tukey HSD comparisons at the final time point (* = $p < 0.05$, ** = $p < 0.01$, *** = $p < 0.001$).

(D) Kaplan-Meier curve of mouse survival over the course of the experiment. Survival was tracked for individual animals until either death or progression to a moribund state.

(E) Representative immunohistochemistry of CPT1A in sectioned tissue following brain perfusion. Each image represents a different animal, 3 animals per group. Scale bar, 100 μm.

ETOM resulted in diminished overall culture growth for all gliomasphere lines tested (Figure 4A). This analysis yielded no significant differences with regard to TCGA classification, IDH1 mutant status, PTEN deficiency, EGFR amplification, or the presence of the EGFRviii mutation (data not shown). Interestingly, ETOM treatment did not inhibit the growth of cultured human fetal neurospheres or SVZ-derived mouse neurospheres. This may indicate that FAO is GBM-specific, irrespective of mutational status, and less important to healthy tissue, making it a potentially attractive therapeutic target. A seven-day growth assay in a subset of patient-derived GBM lines of varying mutational status cultured a physiologically relevant level of glucose (2.5 mM) and showed a similar sensitivity to ETOM inhibition of endogenous FAO to what was observed in 25 mM glucose (Figure S3). The effects of ETOM were comparable to CPT1A knockdown in a highly sensitive line, HK301 (Figure 4B). Following a four-day treatment with ETOM we found a significant decrease in actively dividing cells as assessed using bromodeoxyuridine (BrdU) incorporation (Figure 4C), demonstrating the importance of endogenous FAO to the maintenance of cell proliferation even in a GBM line with a mutation that enhances AKT pathway signaling (HK301). In addition to these effects on proliferation we also observed an increase in cell death as measured by annexin V/PI flow cytometry following treatment with ETOM (Figure 4D). In addition, we examined the effect of FA and 3-OHB supplementation on growth of HK157 in 25 mM, 2.5 mM, and 1 mM glucose (Figures 4E and 4F). Similar to U87 cells (Figures 1C and 1D), a significant increase in growth was observed with FA and 3-OHB supplementation in physiologically relevant (2.5 mM) glucose. Taken together, these data support our hypothesis that FAO is a significant contributor to overall GBM metabolism and growth, which is not prevented by PI3K/AKT/mTOR pathway-promoting mutations in our lines, as has been observed in previous studies on glucose dependency and fatty acid utilization in GBM (Buzzai et al., 2005; Yang et al., 2009; Ye et al., 2013).

To determine the effects of our non-calorie-restricted KD on a primary patient-derived cell xenograft model *in vivo*, we implanted a modestly ETOM-sensitive line, HK408, into the striatum and placed the mice on the KD or standard diet after two days. There were no significant differences in tumor growth or animal survival between the two diets (Figures 4G and 4H). To assess the effects of the KD in an immune competent model, we utilized a syngeneic murine model (Núñez et al., 2019). Again, we found no significant benefit of the KD in this model (Figure S4). Thus, of the three cell lines utilized we did not find a therapeutic benefit of the KD in any of the models tested.

LC-MS with Fully Labeled Palmitic Acid in a Primary Cell Line

We utilized LC-MS analysis with fully labeled ^{13}C palmitic acid to characterize the contribution of FAO to the metabolome of patient-derived GBM cells of a different, moderately ETOM sensitive cell line, HK157. Fractional contribution studies revealed that ETOM treatment caused widespread changes in carbon labeling across the metabolome (Figure 5A). Importantly, ETOM resulted in diminished labeling of acetyl-CoA, the end product of FAO, along with an increase in the amount of labeled palmitate within the cell (Figure 5B). Both results confirmed that labeled FAs were taken up and oxidized within the cell. In addition to acetyl-CoA, ETOM treatment also resulted in diminished labeling within the TCA cycle and among metabolites that commonly feed into the TCA cycle such as glutamine, glutamate, and lactate (Figure 5B). Analysis of the relative amounts of metabolites with ETOM treatment did not result in changes to overall acetyl-CoA or palmitate levels. However, ETOM treatment did result in lower relative levels of TCA-associated metabolites, which include alpha-ketoglutarate, citrate, fumarate, glutamine, and glutamate (Figure 5C). A full list of significantly altered metabolites resulting from FAO inhibition with ETOM, with fractional contribution shown in Table 1 and relative amounts shown in Table 2, demonstrates that

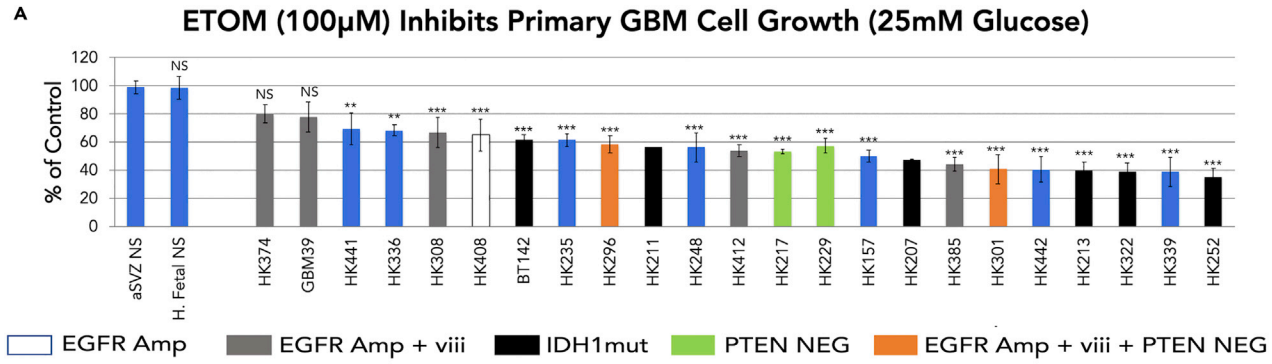
A
ETOM (100μM) Inhibits Primary GBM Cell Growth (25mM Glucose)
% of Control
aSVZ NS
H. Fetal NS
HK374
GBM39
HK441
HK336
HK308
HK408
BT142
HK235
HK296
HK211
HK248
HK412
HK217
HK229
HK157
HK207
HK385
HK301
HK442
HK213
HK322
HK339
HK252
EGFR Amp
EGFR Amp + viii
IDH1mut
PTEN NEG
EGFR Amp + viii + PTEN NEG

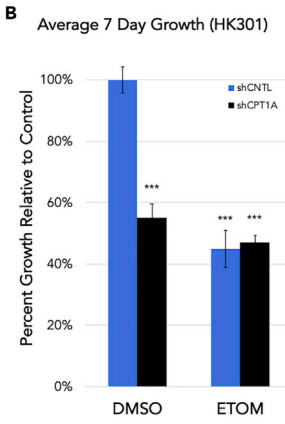
B
Average 7 Day Growth (HK301)
Percent Growth Relative to Control
shCNTL
shCPT1A
DMSO
ETOM

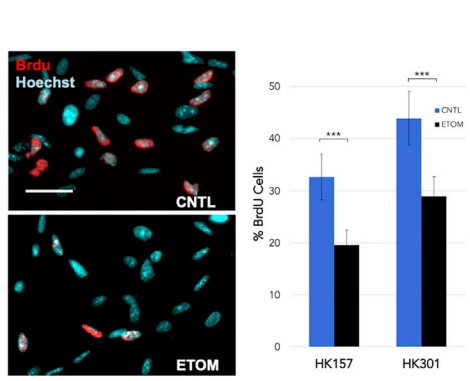
C
Brdu
Hoechst
CNTL
ETOM
% BrdU Cells
HK157
HK301

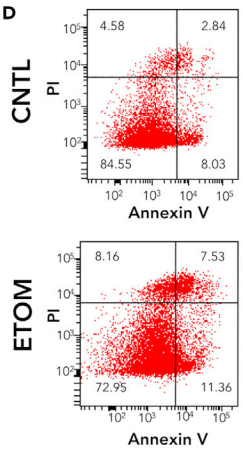
D
CNTL
ETOM
PI
Annexin V
4.58
2.84
84.55
8.03
8.16
7.53
72.95
11.36

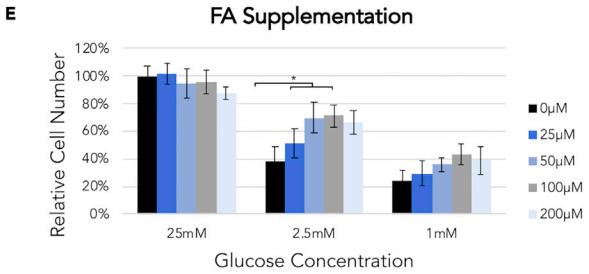
E
FA Supplementation
Relative Cell Number
25mM
2.5mM
1mM
Glucose Concentration
0μM
25μM
50μM
100μM
200μM

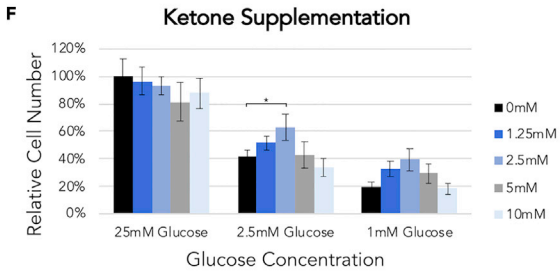
F
Ketone Supplementation
Relative Cell Number
25mM Glucose
2.5mM Glucose
1mM Glucose
Glucose Concentration
0mM
1.25mM
2.5mM
5mM
10mM

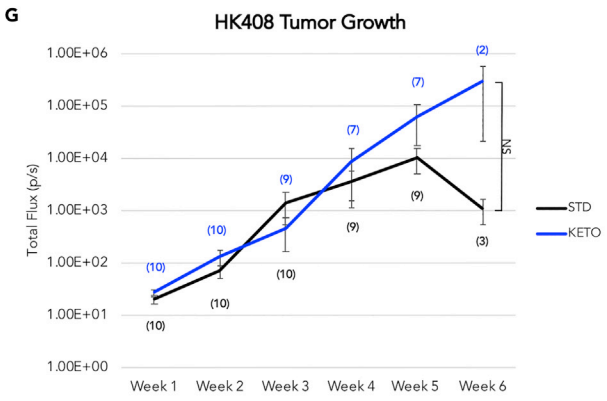
G
HK408 Tumor Growth
Total Flux (p/s)
Week 1
Week 2
Week 3
Week 4
Week 5
Week 6
NS
STD
KETO

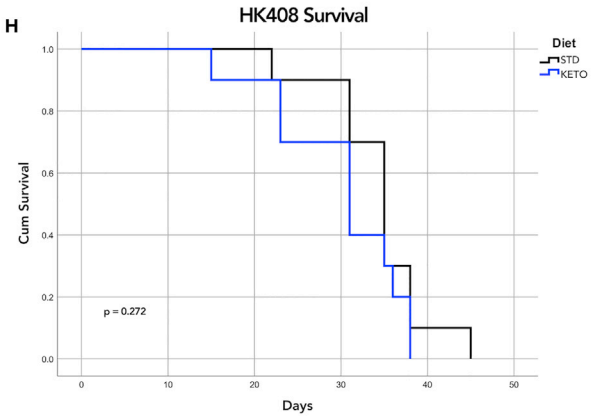
H
HK408 Survival
Cum Survival
p = 0.272
Days
Diet
STD
KETO

Figure 4. Etomoxir Inhibits Patient-derived GBM Cell Proliferation and Promotes Cell Death

(A) Quantification of the effects of 7-day 100 μM ETOM treatment administered twice per week across a panel of patient-derived GBM cell lines and two non-GBM controls (adult-mouse-derived neurospheres and human fetal-derived neurospheres) relative to vehicle-treated controls. n = 3 replicates, except for HK211 and HK207 in which only a single measurement was taken. Error bars = ± SEM. Significance values are relative to aSVZ NS with Bonferroni correction for multiple comparisons. Cultures that are EGFR amplified, EGFR amplified + EGFRviii mutant, IDH1 mutant, and PTEN deficient are indicated. See also Figure S3.

(B) Average 7-day growth of patient-derived cell line HK301with both CPT1A knockdown and 100 μM ETOM. n = 3 replicates. Univariate generalized linear model $F(3,8) = 99.8$, $p = 1.12x10^{-6}$, post-hoc Tukey HSD relative to control (*** = $p < 0.001$).

(C) Assessment of actively dividing cells by BrdU immunocytochemistry in two patient-derived GBM lines grown for 4 days in the presence of 100 μM ETOM. n = 9 replicates. Error bars = ± SEM. Scale bar, 30 μm.

(D) Flow cytometry analysis of cell death using dual Annexin V/PI staining in HK157 cells following 4-day treatment with 100 μM ETOM.

(E and F) (E) Effects of palmitic acid or (F) 3-OHB supplementation at different glucose concentrations on growth of HK157 cells *in vitro*. n = 3 replicates. Error bars = SD. Significance values represent t tests of each condition compared with the control for the same concentration of glucose (* = $p < 0.05$).

(G) Tumor growth measured by bioluminescence imaging for patient-derived cell line HK408. The effect of diet was not statistically significant by mixed effects model ($p > 0.05$). Numbers adjacent to lines indicate N at each time point.

(H) Kaplan-Meier curves for the data as in (E). Diet had no significant effect on survival by Mantel-Cox log rank values ($p = 0.272$).

See also Figure S4.

GBM cells utilize FAO to support a number of critical metabolic pathways throughout the GBM metabolome.

Fatty Acid Oxidation in IDH1 Mutant GBM

Recent studies, including one from our own group (Garrett et al., 2018), have demonstrated that GBMs harboring an IDH1 mutation represent a metabolically distinct subset of glioma. Because of this, we sought to identify potential differences in FAO utilization between our IDH1 mutant and IDH wild-type (WT) gliomasphere cultures. Analysis of microarray data from 67 gliomasphere lines, 7 of which are IDH1 mutant, revealed elevated (although not statistically significant) mRNA expression of *CPT1A* in IDH1 mutant lines compared with IDH WT cultures (Figure 6A). Western blot analysis also showed significantly elevated CPT1A protein expression in three IDH1 mutant lines relative to WT (Figure 6B). Interestingly, although there was a significant decrease in *CPT1C* mRNA expression in IDH1 mutants, we found no difference in protein expression (Figures 6A and 6B). Similar to IDH WT cells, LC-MS analysis with fully labeled palmitic acid in an IDH1 mutant cell line, HK252, showed diminished labeling of acetyl-CoA and several TCA-associated metabolites when treated with ETOM (Figure 6C). Interestingly, 2-hydroxyglutarate (2-HG), a proposed oncometabolite (Dang et al., 2009) and the resulting product of the mutant IDH1 enzyme itself, was among the most heavily labeled metabolite in this patient line. Treatment with ETOM significantly diminished the fractional contribution, suggesting that carbons from FAO are incorporated into the TCA, thus contributing to 2-HG production in IDH1 mutant GBMs. The relative amount of intracellular 2-HG is also reduced with ETOM (Figures 6C and 6D). Interestingly, FAO inhibition with ETOM in IDH1 mutant cells did not result in a decrease in the relative amounts of TCA cycle intermediates as was observed in IDH WT cells (Figure S5), perhaps indicating a greater reliance on FAO to feed the TCA cycle in IDH WT GBM. Analysis of the full list of significantly different metabolites revealed fewer overall metabolites altered by ETOM treatment in IDH1 mutant cells (Table 3 shows fractional contribution and Table 4 shows relative amounts). These data confirm FAO utilization in both IDH1 mutant and WT cells while highlighting several potentially important metabolic differences between the two. Further investigation with a greater number of IDH mutant and WT lines will be needed to fully elucidate these differences.

DISCUSSION

Identifying metabolic vulnerabilities in cancer for use in targeted therapies has been a topic of interest for decades. Although glucose metabolism has drawn the most attention in the scientific community, the ability of brain tumor cells to utilize other substrates for cellular maintenance and bioenergetics has become increasingly evident (Marie and Shinjo, 2011; Salzillo et al., 2016; Seyfried et al., 2011; Woolf et al., 2016). Several lines of evidence exist for the use of a KD to treat brain tumors. The first lies with the innate ability of the human body to efficiently adapt to ketosis (Weber et al., 2018). For example, the KD has been successfully implemented to treat certain diseases such as refractory pediatric epilepsy with no clear sustained adverse health effects (Simeone et al., 2017; Youngson et al., 2017; Zhang et al., 2018). In addition, several previous studies have indicated that many brain tumors lack the ability to oxidize ketones due to decreased expression of several mitochondrial genes (Seyfried et al., 2003; Skinner et al., 2009), although there is also evidence suggesting gliomas oxidize ketone bodies at comparable levels to the brain when exposed to a

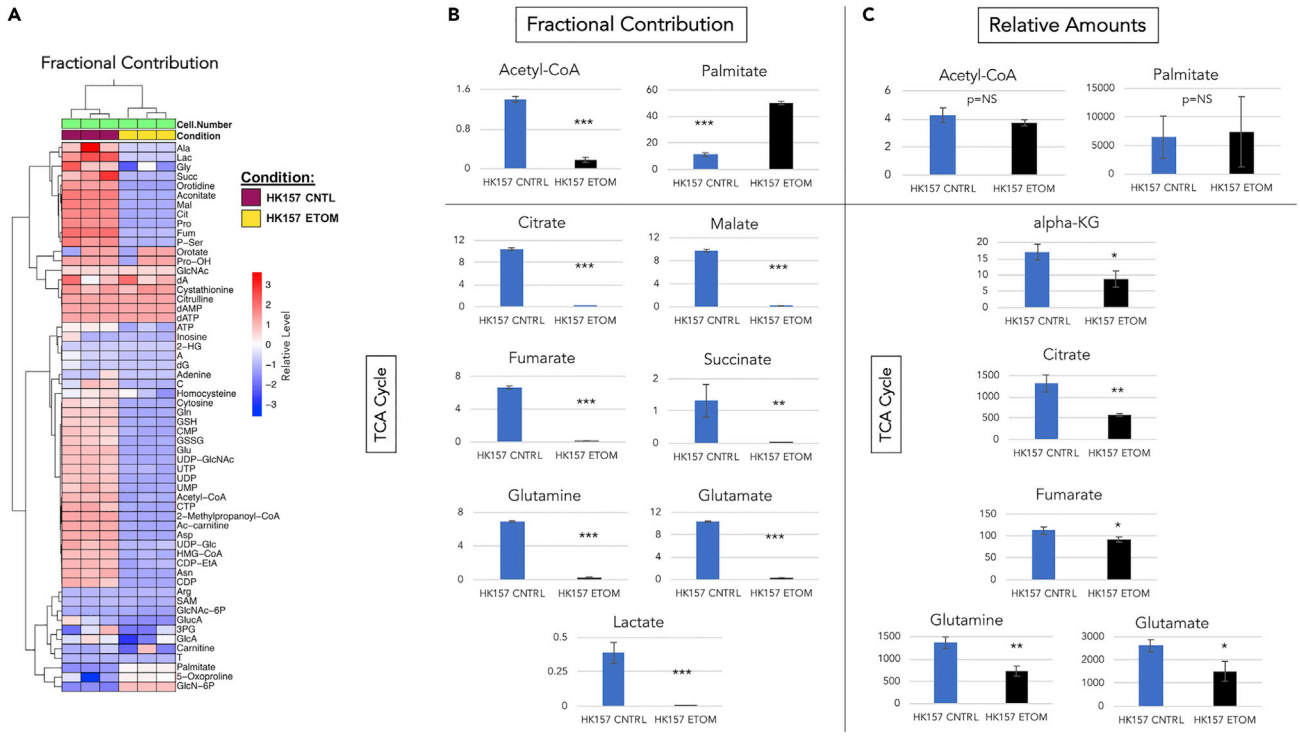

Figure 5. GBM Cells Oxidize FAs to Generate Acetyl-CoA for Use within the TCA Cycle

(A and B) LC-MS analysis of ^{13}C-palmitic acid fractional contribution following treatment with 100 μM ETOM. (A) Heatmap showing effects of ETOM on fractional contribution across metabolites. Relative expression is measured as standard deviations from the group mean. (B) Quantification of the effects of ETOM on intracellular carbon labeling of acetyl-CoA, palmitic acid, and other relevant metabolites associated with the TCA cycle.

(C) Effects of ETOM on relative amounts of relevant metabolites as in (B). ETOM concentration used: 100 μM. n = 3 replicates. Error bars = ± SD (* = $p < 0.05$, ** = $p < 0.01$, *** = $p < 0.001$).

KD (De Feyter et al., 2016). Our study suggests that when glucose levels are diminished, GBM cells may adapt by partially shifting their metabolism toward ketone body and fatty acid oxidation. Prior animal studies investigating the KD have yielded mixed results, usually depending on the manner of administration and ability to achieve ketosis (Lussier et al., 2016; Meidenbauer et al., 2014; Stafford et al., 2010; Zhou et al., 2007). One study using U87 cells in a mouse tumor model found that an *ad libitum* KD increased blood ketone levels without affecting blood glucose or tumor growth (Zhou et al., 2007). Only with a calorie-restricted KD were glucose levels and tumor growth both diminished. This is consistent with studies demonstrating anti-tumor effects of calorie restriction irrespective of the KD (Jiang and Wang, 2013; Mukherjee et al., 2002; Seyfried et al., 2011). Here we report that an *ad libitum* KD significantly elevated blood ketone levels and decreased blood glucose but resulted in a trend for increased tumor growth in the U87 line that was not statistically significant and no effect on tumor growth in a patient-derived GBM line or in a syngeneic mouse tumor. Furthermore, we found for all *in vivo* models used in this study the KD had at best no effect or in the case of U87 cells, a significantly detrimental effect on mouse survival. Although it is possible that the KD in GBM patients may have therapeutic utility, our data suggest that clinical trials investigating such treatments should consider the likelihood that brain tumors will be able to oxidize fatty acids for energy in the absence of additional treatments to modify this capability (Nebeling et al., 1995; Rieger et al., 2014; Schwartz et al., 2015; Zuccoli et al., 2010).

While also investigating ketone body utilization, this study primarily focused on the ability of GBMs to oxidize FAs. Building upon previous reports (Cirillo et al., 2014; Lin et al., 2017; Pike et al., 2011), our results demonstrate that both GBM cell lines and patient-derived GBM cell cultures express the necessary enzymes required for FAO, utilize FAs to support overall metabolism, and inhibition of this process has anti-proliferative effects. Importantly, our results also suggest FAO may be intrinsic to GBM and is not fully counteracted by AKT-enhancing mutations. Activation of the PI3K/AKT/mTOR pathway has been implicated in glucose addiction, a diminished ability to utilize alternative substrates that leaves malignant cells

TCA Cycle	Pentose Phosphate	Nucleotide Metabolism	Amino Acid Metabolism	Fatty Acid/Lipid Metabolism	Currency	Other
Aconitate	S-Adenosyl methionine	5-Methylthio adenosine	L-Asparagine	O-Acetylcarnitine	Acetyl-CoA	D-Glucosamine 6-phosphate[a]
Citrate		Adenosine triphosphate	L-Aspartic acid	Cytidine diphosphate	Adenosine triphosphate	Hydroxymethylglutaryl-CoA
Fumarate		Cytidine	L-Proline	Cytidine diphosphate ethanolamine	Reduced glutathione	
Lactate		Cytidine monophosphate	3-Phosphoserine		Oxidized glutathione	
Malate		Cytidine triphosphate				
Succinate		Cytosine				
L-Glutamine		Hypoxanthine				
L-Glutamate		Orotidine				
		Uridine diphosphate				
		Uridine diphosphate glucose				
		UDP-N-acetylglucosamine				

Table 1. List of all Metabolites Altered by ETOM (100 μM) Treatment with Regard to Fractional Contribution for HK157
Metabolites were measured by labeled ^{13}C-palmitic acid using LC-MS analysis ($p < 0.05$ for all metabolites listed).
[a]Indicates an increase with ETOM treatment.

particularly vulnerable to glucose starvation (Elstrom et al., 2004; Maroon et al., 2015), and a metabolic shift toward FA synthesis (Guo et al., 2009). However, our current study suggests that under physiologically relevant glucose conditions (2.5 mM), FAs play a central role in the overall GBM metabolome regardless of mutational status. A study published during revision of the current manuscript found a difference in use of FAO in tumors based on TGCA classification (Kant et al., 2020). Specifically, FAO was found to be enhanced in mesenchymal tumor lines. However, we observed no such pattern with regard to TCGA subtype in our study. Our findings of a mutation-independent use of FAO may be due to methodological differences with previous studies. Furthermore, our *in vivo* findings that show significantly decreased survival and a trend toward increased U87 tumor growth with a KD support our *in vitro* findings that AKT-enhancing mutations do not make GBMs "glucose addicted," as U87 cells themselves are PTEN deficient. The KD limits glucose availability to the tumor, so the enhanced tumor growth we observe is likely to have been supported by the use of alternative energy substrates despite U87s having PTEN mutations.

The utilization of FAO by these tumors may seem counterintuitive because the brain receives an ample supply of glucose, the most highly utilized substrate in GBM. ATP generation by FAO also demands more oxygen, is a slower overall process, and generates more superoxide than glycolysis (Schönfeld and Reiser, 2013), although it does produce more ATP than glycolysis. Although the idea of simultaneous FA synthesis and oxidation seems counterproductive, studies such as ours make it increasingly clear that FAO makes malignant cells more resilient and adaptable to metabolic stress. FAs represent a readily available substrate that can be utilized to support both bioenergetic demands and for the production of other cellular components. Lipid levels in malignant gliomas are reportedly higher than in normal brain tissues (Srivastava et al., 2010). Gliomas can produce both free FAs and lipid stores endogenously via *de novo* synthesis from excess glucose and via uptake of exogenously produced free FAs from blood. Our experiments suggest that both endogenous and exogenous sources of FAs can be used as an energy substrate to support GBM cell growth. Perhaps the most notable aspect of FAO is that it results in the production of acetyl-CoA, an important metabolite that regulates a number of cellular processes including the TCA cycle.

TCA Cycle	Pentose Phosphate	Nucleotide Metabolism	Amino Acid Metabolism	Fatty Acid/Lipid Metabolism	Currency	Other
α-Keto glutarate	Cystathionine	Adenosine triphosphate	L-Alanine	O-Acetylcarnitine	Adenosine triphosphate	D-Glucosamine 6-phosphate
Citrate	α-D-Glucose 6-phosphate	Deoxyadenosine triphosphate	L-Proline	Phosphocholine	Creatine	4-Hydroxyphenyllactate
Fumarate	Inosine monophosphate[a]	Cytidine diphosphate	L-Serine	Phosphoethanolamine	Reduced nicotinamide adenine dinucleotide	4-OH Phenyl acetic acid
Aconitate	Ribose 5-phosphate	Cytidine triphosphate	L-Threonine		Adenosine monophosphate/ Adenosine triphosphate ratio[a]	L-Ascorbic acid
L-Glutamine		Guanosine triphosphate	L-Citrulline			
L-Glutamate		Uridine triphosphate	2-Methyl-propionyl-CoA			
		Orotidine				
		Cytidine[a]				
		Cytosine[a]				
		Guanosine[a]				

Table 2. List of all Metabolites Altered by ETOM (100 μM) Treatment with Regard to Relative Amounts for HK157
Metabolites were measured by labeled ^{13}C-palmitic acid using LC-MS analysis ($p < 0.05$ for all metabolites listed).
[a]Indicates an increase with ETOM treatment.

Recent evidence demonstrates that much of the acetyl-CoA produced by malignant gliomas is derived from sources other than glucose (Mashimo et al., 2014), highlighting FAO as a potentially critical component of brain tumor metabolism. In addition to ATP, FAO contributes to NADH and NADPH levels. Although labeled carbon from FAO is found throughout the metabolome, it should not contribute net carbons to most metabolites, at least when even-chained FAs are oxidized, as for every two carbons of acetyl-CoA that are metabolized, two carbons are lost as carbon dioxide. However, we found that inhibition of FAO resulted in the loss of relative amounts of a number of metabolites, in addition to fractional contributions, for reasons that are not yet clear, but which may be of use clinically. Interestingly, we found that inhibition of FAO resulted in the loss of relative amounts of some nucleotides, a finding previously reported for endothelial cells (Schoors et al., 2015).

A recent study reported that GBMs are reliant on FAO to sustain proliferation and that acyl-CoA-binding protein (ACBP) promotes this process by regulating the availability of long-chain fatty-acyl CoAs to the mitochondria (Duman et al., 2019). Our results provide further mechanistic insight by identifying CPT1A as a valid therapeutic target and demonstrating that inhibition of CPT1-mediated FAO decreased tumor growth and improved survival using a murine orthotopic xenograft model. In support of this idea, a recent study showed that systemic administration of ETOM in tumor-bearing mice resulted in a trend toward decreased tumor growth and a significant increase in survival, both of which were amplified when combined with a glycolysis inhibitor (Kant et al., 2020). Although the KD initiates production of ketone bodies, it also results in increased FA availability with the potential to be taken up and utilized by the tumor (Fraser et al., 2003; Taha et al., 2005). Because CPT1A knockdown decreased tumor growth from the KD, our results implicate FAs, rather than ketone bodies, as the primary metabolic substrates responsible for the growth-promoting effects of the KD. These results provide strong evidence that FAO is a significant pathway in GBM and may serve as a valuable target either alone or in combination with other currently investigated treatments.

Our study focused on the CPT1A isoform and did not directly study the roles of the CPT1B and C isoforms. This was because the effects of etomoxir were largely mimicked by CPT1A knockdown. CPT1C is found in

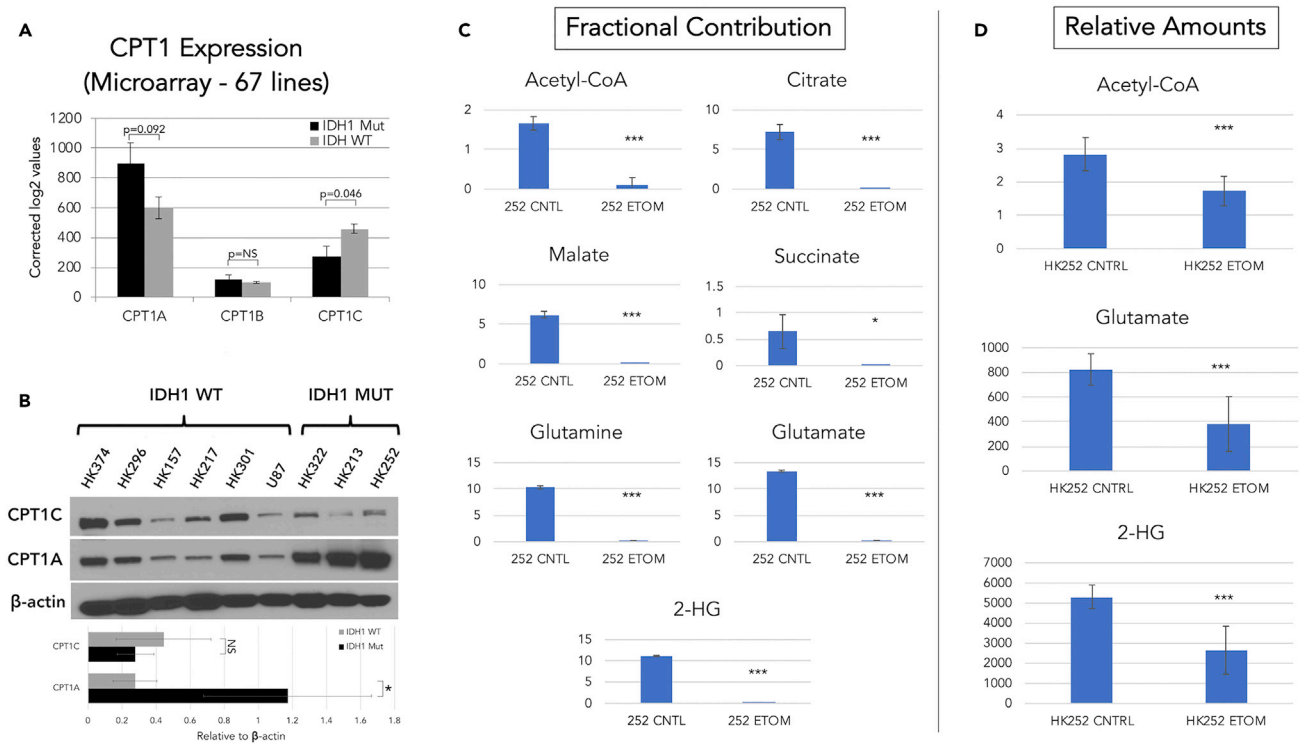

Figure 6. IDH1 Mutant GBM Cells Express Higher Levels of CPT1A and Utilize Fatty Acids to Produce 2-HG

(A) mRNA expression of *CPT1* isoforms in IDH1 mutant (N = 5) and WT (N = 62) patient-derived GBM cultures based on analysis of microarray data.

(B) Western blot of CPT1A and CPT1C across a panel of IDH WT and IDH1 mutant lines. Error bars = ± SD (* = $p < 0.05$, Kruskal-Wallis).

(C and D) Analysis of the effects of ETOM (100 μM) in an IDH1 mutant cell line on fractional contribution and relative amounts of relevant metabolites using ^{13}C-palmitic acid LC-MS. n = 3 replicates. Error bars = ± SD (* = $p < 0.05$, ** = $p < 0.01$, *** = $p < 0.001$).

See also Figure S5.

the brain, and prior studies indicate that it plays important functional roles in tumors outside the brain (Chen et al., 2017; Sanchez-Macedo et al., 2013; Wang et al., 2018; Zaugg et al., 2011), although its role in gliomas is unknown and its precise functional role in FAO is also unclear. *CPT1B* is expressed at low levels in brain tumors, but it too could play a role in GBM FAO. A combinatorial knockout approach, although challenging, would shed light on the contributions of these other enzymes.

Although investigating FA metabolism in GBM as a whole, we also sought to characterize potential differences between IDH1 mutant and WT GBM cells. Recent evidence suggests that GBMs harboring IDH mutations represent a distinct subclass of glioma (Cancer Genome Atlas Research Network, 2015). Our group previously demonstrated IDH1 mutant gliomaspheres are metabolically distinguishable from their WT counterparts based on expression profiles, glucose consumption, and nucleotide synthesis utilization (Garrett et al., 2018). The results of the current study suggest further metabolic differences with regard to FAO. Analysis of CPT1 isoform expression revealed a trend for increased expression of CPT1A in IDH1 mutant cultures relative to IDH WT that was not statistically significant. LC-MS tracing experiments with ^{13}C-palmitic acid revealed extensive FA utilization throughout the metabolomes of both IDH1 mutant and WT cells. However, the effects of FAO inhibition with ETOM were more pronounced within the TCA cycle of IDH WT cells. Importantly, 2-HG was among the most heavily labeled metabolites in IDH1 mutant cells. Treatment with ETOM significantly decreased the amount of 2-HG, indicating that biproducts of FAO may serve as a vital component for the production of this oncometabolite. Although these effects were only tested in a single IDH1 mutant cell line, and thus require further investigation, our results suggest FAO represents an additional mechanism contributing to the unique metabolic phenotype of IDH mutant gliomas.

Although our findings emphasize the complex and highly adaptable nature of brain tumor metabolism, important aspects of these studies require further investigation. The preponderance of evidence reported

TCA Cycle	Nucleotide Metabolism	Amino Acid Metabolism	Fatty Acid/Lipid Metabolism	Currency	Other
Aconitate	Adenosine	L-Asparagine	O-Acetylcarnitine	Acetyl-CoA	N-Acetyl-D-glucosamine 6-phosphate
Citrate	Adenine	L-Aspartic acid	Cytidine diphosphate	Adenosine triphosphate	
Malate	Adenosine triphosphate	L-Arginine[a]	Cytidine diphosphate ethanolamine	Reduced Glutathione	
Succinate	Cytidine	Homocysteine		Oxidized Glutathione	
2-Hydroxyglutarate	Cytidine monophosphate	L-Proline			
L-Glutamine	Cytidine triphosphate				
L-Glutamate	Cytosine				
	Deoxyguanosine				
	Inosine				
	Orotidine				
	Uridine diphosphate				
	Uridine diphosphate glucose				
	UDP-N-acetylglucosamine				
	Uridine monophosphate				
	Uridine triphosphate				

Table 3. List of all Metabolites Altered by ETOM (100 μM) Treatment with Regard to Fractional Contribution for IDH1 Mutant HK252

Metabolites were measured by labeled ^{13}C-palmitic acid using LC-MS analysis ($p < 0.05$ for all metabolites listed).
[a]Indicates an increase with ETOM treatment.

in this study support the conclusion that GBMs oxidize FAs. Inhibition of FAO resulted in overall deficits in cellular growth and FA-mediated mitochondrial respiration. However, although FA supplementation under physiologically relevant glucose concentrations demonstrated inverse effects to that of inhibition in some cell lines, including U87, this effect was not consistent across all patient-derived cell lines tested, suggesting some variability in the ability of GBMs to utilize exogenous FA. Our LC-MS studies also clearly show that FAs are taken up, oxidized, and utilized throughout the GBM metabolome. Finally, many of the effects of FAO inhibition achieved with ETOM were validated using multiple methods of CPT1A knockdown, indicating that they are not due to off-target effects of ETOM. The fact that ETOM has been shown to exhibit off-target effects in certain cells at high doses cannot be overlooked and could ultimately limit its use clinically. Developing more potent and specific FAO inhibitors could prove essential for targeting brain tumors in patients. However, due to the grim prognosis associated with glioma and the currently inadequate treatment options available, this study highlights several important aspects of brain tumor metabolism that have direct application to improving current standard of care therapy.

TCA Cycle	Nucleotide Metabolism	Amino Acid Metabolism	Currency	Other
2-Hydroxyglutarate	Adenine[a]	2-Methylpropanoyl-CoA	Acetyl-CoA	D-Fructose 1,6-bisphosphate
L-Glutamate	Deoxyadenine[a]	Glycine	Creatine	α-D-Glucose 6-phosphate
	Guanosine monophosphate		Reduced nicotinamide adenine dinucleotide	D-Glucosamine 6-phosphate
	Inosine[a]			Pantothenate
	Orotate[a]			Sorbitol

Table 4. List of all Metabolites Altered by ETOM (100 μM) Treatment with Regard to Relative Amounts for IDH1 Mutant HK252

Metabolites were measured by labeled ^{13}C-palmitic acid using LC-MS analysis ($p < 0.05$ for all metabolites listed).
[a]Indicates an increase with ETOM treatment.

Limitations of the Study

The provenance of the U87 cell line has been lost and therefore may not be representative of patient GBMs, although it has been verified as a glioblastoma cell line (Allen et al., 2016). This limitation is somewhat mitigated by our observations in a large array of primary GBM lines *in vitro* and one primary GBM line *in vivo*. A modestly high concentration of ETOM (100 μM) was used for experiments described, allowing the possibility for off-target effects of the drug, which were mitigated at least partially by the observation that the effects of ETOM were largely mimicked by CPT1A knockdown. Our data suggest that CPT1A is the isoform primarily responsible for FAO in GBM; however, we do not know the extent of potential compensation from the B and C isoforms when CPT1A is knocked down. The ketogenic diet used in our *in vivo* models was calorie unrestricted. Although we did observe a decrease in blood glucose and an increase in ketones, there might be more of an effect on tumor growth in an unrestricted ketogenic diet model. In addition, the time frame for the ketogenic diet in these experiments was limited due to the fast rate of growth of the tumors. A longer-term ketogenic diet, such as that which a tumor patient would undergo, might be more effective at slow tumor growth as cellular building blocks become more scarce over time. The metabolomics of FAO inhibition are described in three cell lines (U87, HK157, HK252) and therefore may not be representative of all GBM.

Resource Availability

Lead Contact

Further information and requests for resources and reagents should be directed to and will be fulfilled by the Lead Contact, Harley I. Kornblum, M.D. Ph.D. (hkornblum@mednet.ucla.edu).

Materials Availability

No new or unique materials were generated by this study.

Data and Code Availability

The raw data for the U87 metabolomics presented in Figure 2 can be found at DryadData.org titled "Isotopologue distributions of fatty acid oxidation inhibition in U87 glioma cells" https://doi.org/10.5068/D1R95W.

METHODS

All methods can be found in the accompanying Transparent Methods supplemental file.

SUPPLEMENTAL INFORMATION

Supplemental Information can be found online at https://doi.org/10.1016/j.isci.2020.101453.

ACKNOWLEDGMENTS

This work was supported in whole or part by National Institutes of Health (NIH) Grants: NS052563 (H.I.K.) and CA179071 (A.L.) the UCLA SPORE in Brain Cancer (P50 CA211015); and the Dr. Miriam and Sheldon G. Adelson Medical Research Foundation (H.I.K.). Thanks go to the UCLA Institute for Digital Research and Education for statistical consultation.

AUTHOR CONTRIBUTIONS

Jantzen Sperry: Conceptualization, Methodology, Formal Analysis, Investigation, Writing—Original Draft, Writing—Reviewing & Editing, Michael C. Condro: Conceptualization, Methodology, Formal Analysis, Investigation, Writing Reviewing & Editing, Lea Guo: Investigation, Methodology, Daniel Braas: Methodology, Investigation, Data Curation, Writing—Original Draft, Writing—Reviewing and Editing, Nathan Vanderveer-Harris: Investigation, Kristen K.O. Kim: Investigation, Whitney B. Pope: Supervision, Writing—Reviewing & Editing, Funding Acquisition, Ajit S. Divakaruni: Conceptualization, Methodology, Writing—Reviewing & Editing, Validation, Albert Lai: Conceptualization, Writing—Reviewing & Editing, Heather Christofk: Conceptualization, Supervision, Writing—Reviewing & Editing, Maria G. Castro: Resources, Writing—Reviewing & Editing, Pedro R. Lowenstein: Resources, Writing—Reviewing & Editing, Janel E. Le Belle: Conceptualization, Methodology, Validation, Writing—Original Draft, Writing—Reviewing & Editing, Supervision, Harley I. Kornblum: Conceptualization, Resources, Writing—Original Draft, Writing—Review & Editing, Supervision, Project Administration, Funding Acquisition.

DECLARATION OF INTERESTS

The authors declare no competing interests.

Received: December 27, 2019
Revised: June 28, 2020
Accepted: August 10, 2020
Published: September 25, 2020

REFERENCES

Abdelwahab, M.G., Fenton, K.E., Preul, M.C., Rho, J.M., Lynch, A., Stafford, P., and Scheck, A.C. (2012). The ketogenic diet is an effective adjuvant to radiation therapy for the treatment of malignant glioma. PLoS One *7*, e36197.

Agnihotri, S., and Zadeh, G. (2016). Metabolic reprogramming in glioblastoma: the influence of cancer metabolism on epigenetics and unanswered questions. Neuro Oncol. *18*, 160–172.

Allen, M., Bjerke, M., Edlund, H., Nelander, S., and Westermark, B. (2016). Origin of the U87MG glioma cell line: good news and bad news. Sci. Transl. Med. *8*, 354re3.

Buzzai, M., Bauer, D.E., Jones, R.G., Deberardinis, R.J., Hatzivassiliou, G., Elstrom, R.L., and Thompson, C.B. (2005). The glucose dependence of Akt-transformed cells can be reversed by pharmacologic activation of fatty acid beta-oxidation. Oncogene *24*, 4165–4173.

Cancer Genome Atlas Research Network (2015). Comprehensive, integrative genomic analysis of diffuse lower-grade gliomas. N. Engl. J. Med. *372*, 2481–2498.

Chen, Y., Wang, Y., Huang, Y., Zeng, H., Hu, B., Guan, L., Zhang, H., Yu, A.M., Johnson, C.H., Gonzalez, F.J., et al. (2017). PPARα regulates tumor cell proliferation and senescence via a novel target gene carnitine palmitoyltransferase 1C. Carcinogenesis *38*, 474–483.

Cirillo, A., Di Salle, A., Petillo, O., Melone, M.A.B., Grimaldi, G., Bellotti, A., Torelli, G., De' Santi, M.S., Cantatore, G., Marinelli, A., et al. (2014). High grade glioblastoma is associated with aberrant expression of ZFP57, a protein involved in gene imprinting, and of CPT1A and CPT1C that regulate fatty acid metabolism. Cancer Biol. Ther. *15*, 735–741.

Dang, L., White, D.W., Gross, S., Bennett, B.D., Bittinger, M.A., Driggers, E.M., Fantin, V.R., Jang, H.G., Jin, S., Keenan, M.C., et al. (2009). Cancer-associated IDH1 mutations produce 2-hydroxyglutarate. Nature *462*, 739–744.

Darmanis, S., Sloan, S.A., Croote, D., Mignardi, M., Chernikova, S., Samghababi, P., Zhang, Y., Neff, N., Kowarsky, M., Caneda, C., et al. (2017). Single-cell RNA-seq analysis of infiltrating neoplastic cells at the migrating front of human glioblastoma. Cell Rep. *21*, 1399–1410.

De Feyter, H.M., Behar, K.L., Rao, J.U., Madden-Hennessey, K., Ip, K.L., Hyder, F., Drewes, L.R., Geschwind, J.F., de Graaf, R.A., and Rothman, D.L. (2016). A ketogenic diet increases transport and oxidation of ketone bodies in RG2 and 9L gliomas without affecting tumor growth. Neuro Oncol. *18*, 1079–1087.

Duman, C., Yaqubi, K., Hoffmann, A., Acikgöz, A.A., Korshunov, A., Bendszus, M., Herold-Mende, C., Liu, H.K., and Alfonso, J. (2019). Acyl-CoA-binding protein drives glioblastoma tumorigenesis by sustaining fatty acid oxidation. Cell Metab. *30*, 274–289e5.

Elstrom, R.L., Bauer, D.E., Buzzai, M., Karnauskas, R., Harris, M.H., Plas, D.R., Zhuang, H., Cinalli, R.M., Alavi, A., Rudin, C.M., and Thompson, C.B. (2004). Akt stimulates aerobic glycolysis in cancer cells. Cancer Res. *64*, 3892–3899.

Fraser, D.D., Whiting, S., Andrew, R.D., Macdonald, E.A., Musa-Veloso, K., and Cunnane, S.C. (2003). Elevated polyunsaturated fatty acids in blood serum obtained from children on the ketogenic diet. Neurology *60*, 1026–1029.

Furuta, E., Pai, S.K., Zhan, R., Bandyopadhyay, S., Watabe, M., Mo, Y.-Y., Hirota, S., Hosobe, S., Tsukada, T., Miura, K., et al. (2008). Fatty acid synthase gene is up-regulated by hypoxia via activation of Akt and sterol regulatory element binding protein-1. Cancer Res. *68*, 1003–1011.

Garrett, M., Sperry, J., Braas, D., Yan, W., Le, T.M., Mottahedeh, J., Ludwig, K., Eskin, A., Qin, Y., Levy, R., et al. (2018). Metabolic characterization of isocitrate dehydrogenase (IDH) mutant and IDH wildtype gliomaspheres uncovers cell type-specific vulnerabilities. Cancer Metab. *6*, 4.

Guo, D., Prins, R.M., Dang, J., Kuga, D., Iwanami, A., Soto, H., Lin, K.Y., Huang, T.T., Akhavan, D., Hock, M.B., et al. (2009). EGFR signaling through an Akt-SREBP-1-dependent, rapamycin-resistant pathway sensitizes glioblastomas to antilipogenic therapy. Sci. Signal. *2*, ra82.

Jiang, Y.-S., and Wang, F.-R. (2013). Caloric restriction reduces edema and prolongs survival

in a mouse glioma model. J. Neurooncol. *114*, 25–32.

Kant, S., Kesarwani, P., Prabhu, A., Graham, S.F., Buelow, K.L., Nakano, I., and Chinnaiyan, P. (2020). Enhanced fatty acid oxidation provides glioblastoma cells metabolic plasticity to accommodate to its dynamic nutrient microenvironment. Cell Death Dis. *11*, 253.

Kim, J.W., Tchernyshyov, I., Semenza, G.L., and Dang, C.V. (2006). HIF-1-mediated expression of pyruvate dehydrogenase kinase: a metabolic switch required for cellular adaptation to hypoxia. Cell Metab. *3*, 177–185.

Lee, E., Yong, R.L., Paddison, P., and Zhu, J. (2018). Comparison of glioblastoma (GBM) molecular classification methods. Semin. Cancer Biol. *53*, 201–211.

Lin, H., Patel, S., Affleck, V.S., Wilson, I., Turnbull, D.M., Joshi, A.R., Maxwell, R., and Stoll, E.A. (2017). Fatty acid oxidation is required for the respiration and proliferation of malignant glioma cells. Neuro Oncol. *19*, 43–54.

Lopes-Cardozo, M., Larsson, O.M., and Schousboe, A. (1986). Acetoacetate and glucose as lipid precursors and energy substrates in primary cultures of astrocytes and neurons from mouse cerebral cortex. J. Neurochem. *46*, 773–778.

Lussier, D.M., Woolf, E.C., Johnson, J.L., Brooks, K.S., Blattman, J.N., and Scheck, A.C. (2016). Enhanced immunity in a mouse model of malignant glioma is mediated by a therapeutic ketogenic diet. BMC Cancer *16*, 310.

Marie, S.K.N., and Shinjo, S.M.O. (2011). Metabolism and brain cancer. Clinics (Sao Paulo) *66* (*Suppl 1*), 33–43.

Maroon, J.C., Seyfried, T.N., Donohue, J.P., and Bost, J. (2015). The role of metabolic therapy in treating glioblastoma multiforme. Surg. Neurol. Int. *6*, 61.

Mashimo, T., Pichumani, K., Vemireddy, V., Hatanpaa, K.J., Singh, D.K., Sirasanagandla, S., Nannepaga, S., Piccirillo, S.G., Kovacs, Z., Foong, C., et al. (2014). Acetate is a bioenergetic substrate for human glioblastoma and brain metastases. Cell *159*, 1603–1614.

Maurer, G.D., Brucker, D.P., Bähr, O., Harter, P.N., Hattingen, E., Walenta, S., Mueller-Klieser, W., Steinbach, J.P., and Rieger, J. (2011). Differential utilization of ketone bodies by neurons and glioma cell lines: a rationale for ketogenic diet as experimental glioma therapy. BMC Cancer *11*, 315.

Meidenbauer, J.J., Ta, N., and Seyfried, T.N. (2014). Influence of a ketogenic diet, fish-oil, and calorie restriction on plasma metabolites and lipids in C57BL/6J mice. Nutr. Metab. (Lond) *11*, 23.

Mukherjee, P., El-Abbadi, M.M., Kasperzyk, J.L., Ranes, M.K., and Seyfried, T.N. (2002). Dietary restriction reduces angiogenesis and growth in an orthotopic mouse brain tumour model. Br. J. Cancer *86*, 1615–1621.

Mukherjee, P., Augur, Z.M., Li, M., Hill, C., Greenwood, B., Domin, M.A., Kondakci, G., Narain, N.R., Kiebish, M.A., Bronson, R.T., et al. (2019). Therapeutic benefit of combining calorie-restricted ketogenic diet and glutamine targeting in late-stage experimental glioblastoma. Commun. Biol. *2*, 200.

Nebeling, L.C., Miraldi, F., Shurin, S.B., and Lerner, E. (1995). Effects of a ketogenic diet on tumor metabolism and nutritional status in pediatric oncology patients: two case reports. J. Am. Coll. Nutr. *14*, 202–208.

Núñez, F.J., Mendez, F.M., Kadiyala, P., Alghamri, M.S., Savelieff, M.G., Garcia-Fabiani, M.B., Haase, S., Koschmann, C., Calinescu, A.A., Kamran, N., et al. (2019). IDH1-R132H acts as a tumor suppressor in glioma via epigenetic up-regulation of the DNA damage response. Sci. Transl. Med. *11*, eaaq1427.

Park, H.R., Kim, J.-Y., Park, K.-Y., and Lee, J. (2011). Lipotoxicity of palmitic acid on neural progenitor cells and hippocampal neurogenesis. Toxicol. Res. *27*, 103–110.

Pike, L.S., Smift, A.L., Croteau, N.J., Ferrick, D.A., and Wu, M. (2011). Inhibition of fatty acid oxidation by etomoxir impairs NADPH production and increases reactive oxygen species resulting in ATP depletion and cell death in human glioblastoma cells. Biochim. Biophys. Acta *1807*, 726–734.

Poff, A.M., Ari, C., Arnold, P., Seyfried, T.N., and D'Agostino, D.P. (2014). Ketone supplementation decreases tumor cell viability and prolongs survival of mice with metastatic cancer. Int. J. Cancer *135*, 1711–1720.

Rieger, J., Bähr, O., Maurer, G.D., Hattingen, E., Franz, K., Brucker, D., Walenta, S., Kämmerer, U., Coy, J.F., Weller, M., and Steinbach, J.P. (2014). ERGO: a pilot study of ketogenic diet in recurrent glioblastoma. Int. J. Oncol. *44*, 1843–1852.

Salzillo, T.C., Hu, J., Nguyen, L., Whiting, N., Lee, J., Weygand, J., Dutta, P., Pudakalakatti, S., Millward, N.Z., Gammon, S.T., et al. (2016). Interrogating metabolism in brain cancer. Magn. Reson. Imaging Clin. N. Am. *24*, 687–703.

Sanchez-Macedo, N., Feng, J., Faubert, B., Chang, N., Elia, A., Rushing, E.J., Tsuchihara, K., Bungard, D., Berger, S.L., Jones, R.G., et al. (2013). Depletion of the novel p53-target gene carnitine palmitoyltransferase 1C delays tumor growth in the neurofibromatosis type I tumor model. Cell Death Differ. *20*, 659–668.

Schönfeld, P., and Reiser, G. (2013). Why does brain metabolism not favor burning of fatty acids to provide energy? Reflections on disadvantages of the use of free fatty acids as fuel for brain. J. Cereb. Blood Flow Metab. *33*, 1493–1499.

Schoors, S., Bruning, U., Missiaen, R., Queiros, K.C., Borgers, G., Elia, I., Zecchin, A., Cantelmo, A.R., Christen, S., Goveia, J., et al. (2015). Fatty acid carbon is essential for dNTP synthesis in endothelial cells. Nature *526*, 144.

Schwartz, K., Chang, H.T., Nikolai, M., Pernicone, J., Rhee, S., Olson, K., Kurniali, P.C., Hord, N.G., and Noel, M. (2015). Treatment of glioma patients with ketogenic diets: report of two cases treated with an IRB-approved energy-restricted ketogenic diet protocol and review of the literature. Cancer Metab. *3*, 3.

Seyfried, T.N., Kiebish, M.A., Marsh, J., Shelton, L.M., Huysentruyt, L.C., and Mukherjee, P. (2011). Metabolic management of brain cancer. Biochim. Biophys. Acta *1807*, 577–594.

Seyfried, T.N., Sanderson, T.M., El-Abbadi, M.M., McGowan, R., and Mukherjee, P. (2003). Role of glucose and ketone bodies in the metabolic control of experimental brain cancer. Br. J. Cancer *89*, 1375–1382.

Silver, I.A., and Erecińska, M. (1994). Extracellular glucose concentration in mammalian brain: continuous monitoring of changes during increased neuronal activity and upon limitation in oxygen supply in normo-, hypo-, and hyperglycemic animals. J. Neurosci. *14*, 5068–5076.

Simeone, T.A., Matthews, S.A., Samson, K.K., and Simeone, K.A. (2017). Regulation of brain PPARgamma2 contributes to ketogenic diet anti-seizure efficacy. Exp. Neurol. *287*, 54–64.

Skinner, R., Trujillo, A., Ma, X., and Beierle, E.A. (2009). Ketone bodies inhibit the viability of human neuroblastoma cells. J. Pediatr. Surg. *44*, 212–216, discussion 216.

Srivastava, N.K., Pradhan, S., Gowda, G.A.N., and Kumar, R. (2010). In vitro, high-resolution 1H and 31P NMR based analysis of the lipid components in the tissue, serum, and CSF of the patients with primary brain tumors: one possible diagnostic view. NMR Biomed. *23*, 113–122.

Stafford, P., Abdelwahab, M.G., Kim, D.Y., Preul, M.C., Rho, J.M., and Scheck, A.C. (2010). The ketogenic diet reverses gene expression patterns and reduces reactive oxygen species levels when used as an adjuvant therapy for glioma. Nutr. Metab. (Lond) *7*, 74.

Strickland, M., and Stoll, E.A. (2017). Metabolic reprogramming in glioma. Front. Cell Dev. Biol. *5*, 43.

Taha, A.Y., Ryan, M.A.A., and Cunnane, S.C. (2005). Despite transient ketosis, the classic high-fat ketogenic diet induces marked changes in fatty acid metabolism in rats. Metab. Clin. Exp. *54*, 1127–1132.

Vander Heiden, M.G., Cantley, L.C., and Thompson, C.B. (2009). Understanding the Warburg effect: the metabolic requirements of cell proliferation. Science *324*, 1029–1033.

Vidali, S., Aminzadeh, S., Lambert, B., Rutherford, T., Sperl, W., Kofler, B., and Feichtinger, R.G. (2015). Mitochondria: the ketogenic diet–A metabolism-based therapy. Int. J. Biochem. Cell Biol. *63*, 55–59.

Wang, Y., Chen, Y., Guan, L., Zhang, H., Huang, Y., Johnson, H., Wu, Z., Gonzalez, F.J., Yu, A., Huang, P., et al. (2018). Carnitine palmitoyltransferase 1C regulates cancer cell senescence through mitochondria-associated metabolic reprogramming. Cell Death Differ. *25*, 735–748.

Weber, D.D., Aminazdeh-Gohari, S., and Kofler, B. (2018). Ketogenic diet in cancer therapy. Aging (Albany NY) *10*, 164–165.

Weightman Potter, P.G., Vlachaki Walker, J.M., Robb, J.L., Chilton, J.K., Williamson, R., Randall, A.D., Ellacott, K.L.J., and Beall, C. (2019). Basal fatty acid oxidation increases after recurrent low glucose in human primary astrocytes. Diabetologia *62*, 187–198.

Woolf, E.C., Syed, N., and Scheck, A.C. (2016). Tumor metabolism, the ketogenic diet and β-hydroxybutyrate: novel approaches to adjuvant brain tumor therapy. Front. Mol. Neurosci. *9*, 122.

Yang, C., Sudderth, J., Dang, T., Bachoo, R.M., Bachoo, R.G., McDonald, J.G., and DeBerardinis, R.J. (2009). Glioblastoma cells require glutamate dehydrogenase to survive impairments of glucose metabolism or Akt signaling. Cancer Res. *69*, 7986–7993.

Yang, J., Nie, J., Ma, X., Wei, Y., Peng, Y., and Wei, X. (2019). Targeting PI3K in cancer: mechanisms and advances in clinical trials. Mol. Cancer *18*, 26.

Ye, F., Zhang, Y., Liu, Y., Yamada, K., Tso, J.L., Menjivar, J.C., Tian, J.Y., Yong, W.H., Schaue, D., Mischel, P.S., et al. (2013). Protective properties of radio-chemoresistant glioblastoma stem cell clones are associated with metabolic adaptation to reduced glucose dependence. PLoS One *8*, e80397.

Youngson, N.A., Morris, M.J., and Ballard, J.W.O. (2017). The mechanisms mediating the antiepileptic effects of the ketogenic diet, and potential opportunities for improvement with metabolism-altering drugs. Seizure *52*, 15–19.

Zaugg, K., Yao, Y., Reilly, P.T., Kannan, K., Kiarash, R., Mason, J., Huang, P., Sawyer, S.K., Fuerth, B., Faubert, B., et al. (2011). Carnitine palmitoyltransferase 1C promotes cell survival and tumor growth under conditions of metabolic stress. Genes Dev. *25*, 1041–1051.

Zhang, Y., Xu, J., Zhang, K., Yang, W., and Li, B. (2018). The anticonvulsant effects of ketogenic diet on epileptic seizures and potential mechanisms. Curr. Neuropharmacol. *16*, 66–70.

Zhou, W., Mukherjee, P., Kiebish, M.A., Markis, W.T., Mantis, J.G., and Seyfried, T.N. (2007). The calorically restricted ketogenic diet, an effective alternative therapy for malignant brain cancer. Nutr. Metab. (Lond) *4*, 5.

Zuccoli, G., Marcello, N., Pisanello, A., Servadei, F., Vaccaro, S., Mukherjee, P., and Seyfried, T.N. (2010). Metabolic management of glioblastoma multiforme using standard therapy together with a restricted ketogenic diet: case Report. Nutr. Metab. (Lond.) *7*, 33.

iScience, Volume *23*

Supplemental Information

Glioblastoma Utilizes Fatty Acids and Ketone Bodies for Growth Allowing Progression during Ketogenic Diet Therapy

Jantzen Sperry, Michael C. Condro, Lea Guo, Daniel Braas, Nathan Vanderveer-Harris, Kristen K.O. Kim, Whitney B. Pope, Ajit S. Divakaruni, Albert Lai, Heather Christofk, Maria G. Castro, Pedro R. Lowenstein, Janel E. Le Belle, and Harley I. Kornblum

Supplementary Materials:

Supplemental Figures

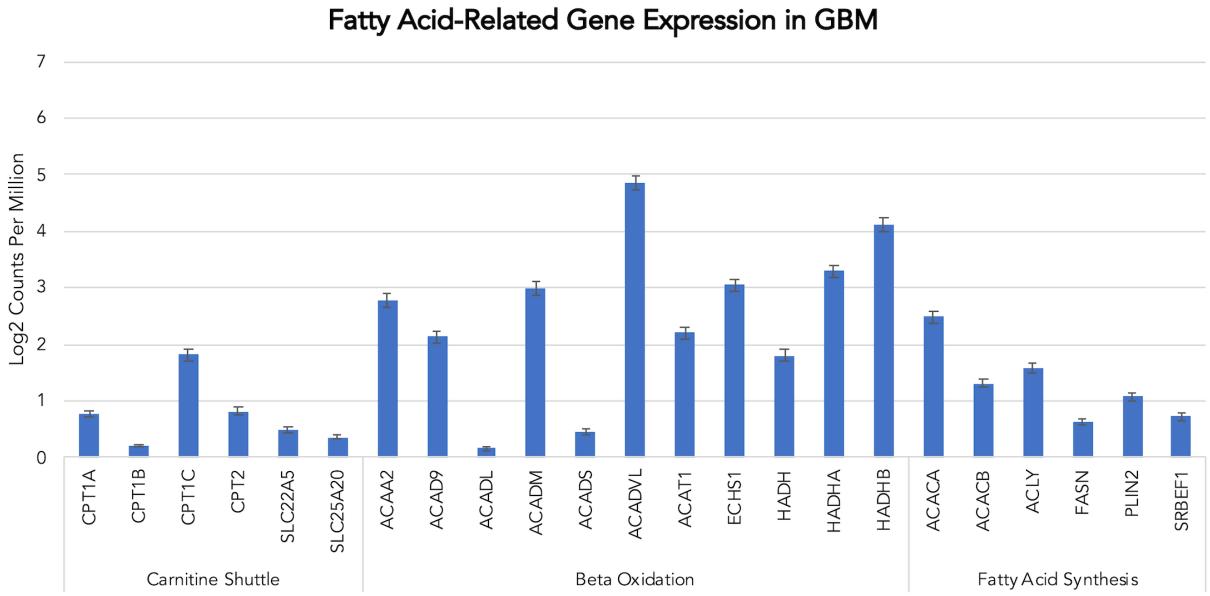

Figure S1: Expression of Fatty Acid-Related Genes in GBM, Related to Figure 1A.

Average expression of genes related to mitochondrial FAO and synthesis by single cell RNAseq from four patients. Data represent expression levels from neoplastic cells found either at the tumor core (n=1029 cells) or in the periphery (n=62 cells). Error bars ± SEM.

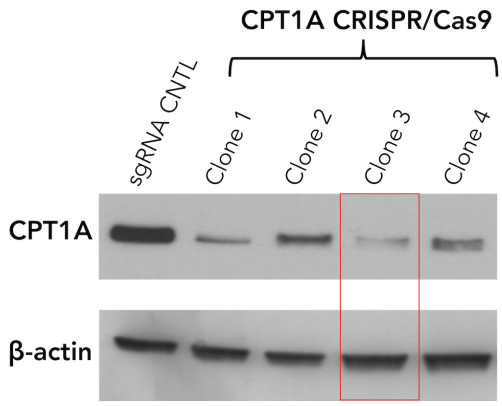

Figure S2: Efficiency of CRISPR/Cas9 targeting CPT1A, Related to Figure 2.

Western blot of lysates from U87 cells expressing Cas9 and either control sgRNA or one of 4 CPT1A-targeting sgRNA clones. Due to its increased efficiency at reducing CPT1A, clone 3 was used in the experiments shown in Figure 2.

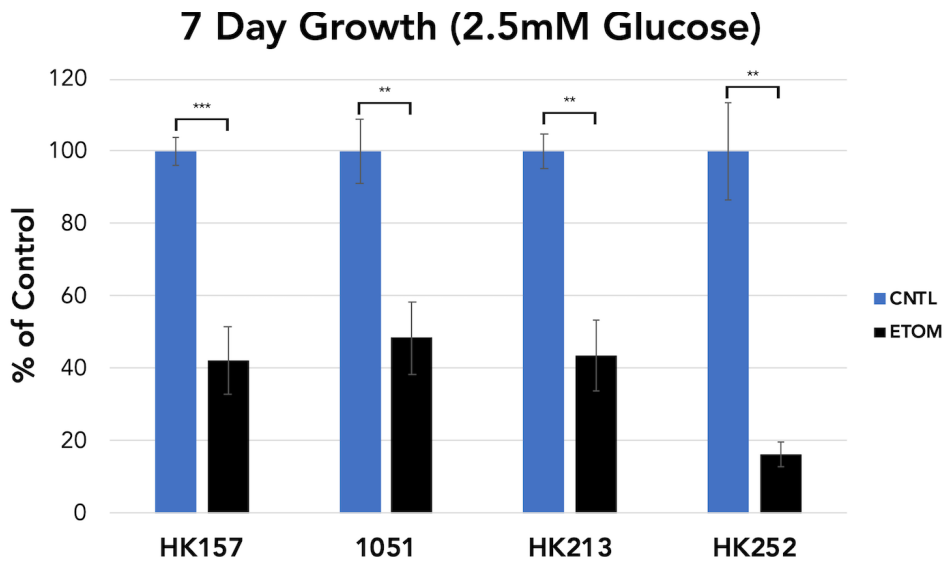

Figure S3: ETOM inhibits growth of patient-derived GBM cell lines in 2.5 mM glucose, but response to FA or 3-OHB supplementation varies, Related to Figure 4A.

7 day growth assessment (cell counts) with 100 μM ETOM, 50 mM palmitate (FA), and 1.25 mM 3-OHB in 2.5 mM glucose. n = 3 replicates. Error bars = ± SD. (* = $p<0.05$, ** = $p<0.01$, *** = $p<0.001$).

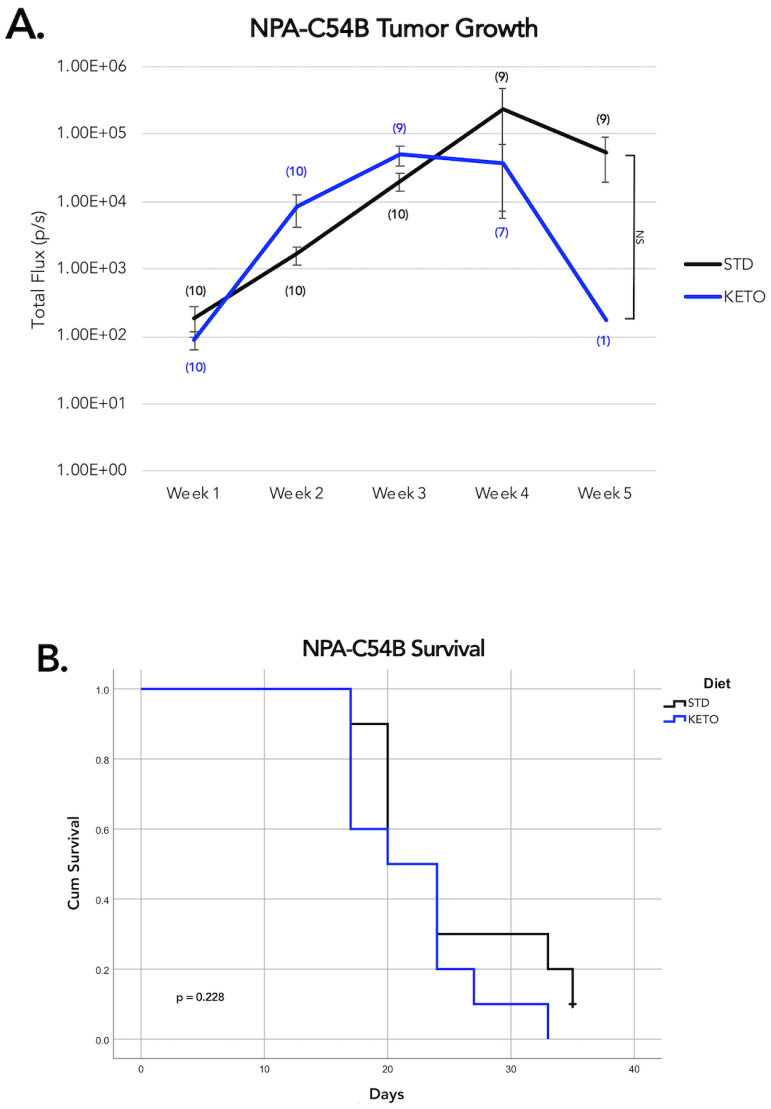

Figure S4: The unrestricted ketogenic diet yields no benefit to tumor growth or survival in a mouse model of GBM, Related to Figure 4E and 4F.

Tumor growth (left) measured by luciferase imaging and survival (right) of a murine model of GBM (NPA-C54B) implanted into immune-competent C57Bl/6 mice. Numbers in parentheses indicate the number of mice averaged for each timepoint. Error bars = ± SEM. (* = $p<0.05$, ** = $p<0.01$, *** = $p<0.001$).

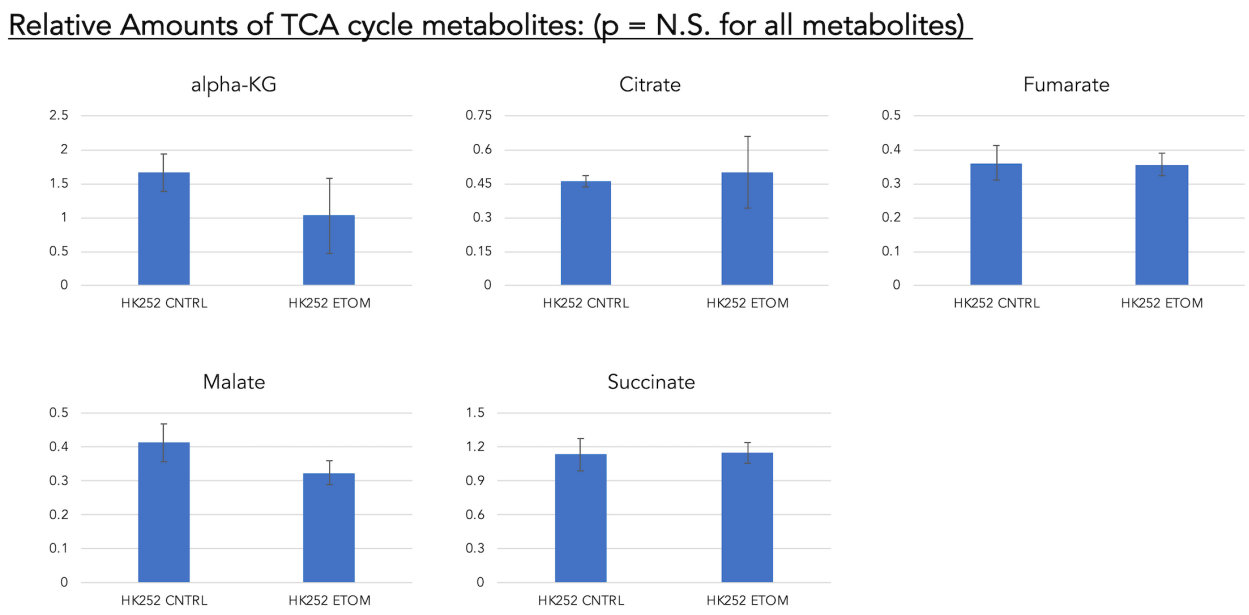

Figure S5: CPT1 inhibition with ETOM does not alter relative amounts of TCA metabolites in IDH1 mutant cells, Related to Figure 6.

Analysis of the effects of 100 μM ETOM on relative amounts of TCA metabolites in an IDH1 mutant line using ^{13}C-palmitic acid (LC-MS). n = 3 replicates. Error bars = ± SD. $p>0.05$ (N.S.) for all metabolites shown.

Transparent Methods:

Collection and Maintenance of *In Vitro* Cultures

Tumor samples were collected under institutional review board-approved protocols and graded by neuropathologists. Patient-derived gliomasphere cultures were prepared as follows: immediately after receiving resected tissue, samples were digested with papain and acellular debris was removed. The remaining cells were incubated in gliomasphere defined media containing DMEM/F-12 supplemented with B27, heparin, EGF, bFGF, and penicillin/streptomycin until sphere formation was achieved. Gliomasphere stocks were frozen down at approximately passage 5 to maintain cells at low passage throughout the study. All cell lines used in this study, including U87, were continuously grown in serum-free gliomasphere media.

Expression Analysis

Relevant expression, mutational status (such as EGFR and IDH1), and patient characteristics for the majority of cell lines used in this study have been previously reported (Laks et al., 2016; Garrett et al., 2018). The following cultures are known to be PTEN deficient: U87, HK217, HK229, HK296, HK301, but there may be other cultures that are PTEN mutated/deleted as well. Also of note, while BT142 is IDH1 mutant (R132H), it does not produce 2-HG (Luchman et al., 2013). HK211 is both IDH1 (R132H) and EGFRviii mutant. Known status of EGFR, PTEN, and IDH1 are indicated in Figure 6A for patient-derived GBM cultures. Analysis of *CPT1* isoform expression is based on the microarray dataset (GSE98995) previously described by Laks et al. 2016 and available in the Gene Expression Omnibus (GEO) repository.

Variable Glucose Media and Substrate Supplementation

All media described contain B27, heparin, EGF, bFGF, and penicillin/streptomycin. For 25 mM glucose the base media used is Neurobasal-A Medium ([-] Glutamine) (Gibco #10888-022) supplemented with GlutaMax Supplement (Gibco #35050061). 2.5 mM and 1 mM glucose media was made by combining the Neurobasal-A Medium ([-] Glutamine) above with Neurobasal-A Medium ([-] D-glucose, [-] Sodium Pyruvate) (Gibco #A24775-01) to achieve the desired glucose concentration. Glutamax Supplement and sodium pyruvate (Gibco #11360-070) were then added to reach a final concentration of 1X. Palmitic acid was purchased from Sigma-Aldrich (#P0500) and conjugated with fatty acid free, low endotoxin bovine serum albumin (BSA, Sigma Aldrich, #A1595). Carnitine (Sigma Aldrich, #C0283) was included in fatty acid-supplemented conditions. 3-hydroxybutyrate (3-OHB) was also purchased from Sigma (#166898).

shRNA and CRISPR/Cas9 Lentiviral Knockdown

Plasmids with shCPT1A (RHS4531-EG1374 glycerol set) and the non-silencing shCNTL (RHS4346) cloned into pGIPZ expression vectors were purchased from Dharmacon. The firefly luciferase-GFP virus (FLuc-GFP; backbone= pRRL-sinCMV-iresGFP) was produced by UCLA Vectorcore and supported by Molecular Technologies Core (IMTC) CURE/P30 DK41301-26. These plasmids were transfected into 293T cells along with 2nd generation viral ΔR8.74 package and VSV-g envelope for production of lentivirus.

U87 In Vivo Orthotopic Xenotransplants

All animal experimentation was performed with institutional approval following NIH guidelines using adult NSG mice. Intracranial xenotransplants were performed similarly to previous descriptions with minor changes (Laks et al., 2009).

CPT1A /Ketogenic Diet:

10^5 U87 cells expressing either shCNTL or shCPT1A along with firefly luciferase-GFP (FLuc-GFP) were stereotactically injected unilaterally into the striatum of NOD *scid* gamma (NSG) mice under isoflurane anesthesia over 5 minutes using the following coordinates: 1.5 mm lateral and 0.5 mm anterior to bregma, and 3.0 mm below the pial surface. N=10 mice per group. As shown in Figure 3B, mice were kept on standard diet for 4 days to allow appropriate recovery, after which half of each group was placed on the ketogenic diet (BioServ, S3666). On Day 8, weekly bioluminescence imaging was initiated as described below. On Day 21 mouse weight, blood glucose and ketone measurements were taken. Tumor growth was measured until each animal either died or became moribund. Mouse survival was tracked for all groups.

HK408 and NPA-C54B :

Transplants and institution of the ketogenic diet for this experiment were carried out as described above with the exception that there was no knockdown of CPT1A group and therefore only 20 total mice were used (10 per group). For HK408, 10^5 cells were implanted into 10 male and 10 female NSG mice, and groups were divided evenly by sex. No sex differences were found with regards to the ketogenic diet (data not shown). In the murine tumor model, $5x10^3$ cells of NPA-C54B were implanted into the striatum of 20 male C57Bl/6 mice as described in Nuñez et al., 2019, at coordinates 1.0 mm anterior and 2.5 mm lateral to bregma, and 2.5 mm deep. These cell lines were chosen because of their consistency in forming tumors that grow quickly. The speed of tumor formation was important, not simply for convenience, but it allowed us to take into account concerns regarding significant weight loss and the overall health of animals receiving a

long-term ketogenic diet. As above, mice were kept on a standard diet for four days after surgery, at which time they were divided into groups of standard and ketogenic diet. Tumor growth was measured by weekly bioluminescence imaging as described above, and survival was tracked until mice died or became moribund.

Bioluminescent Imaging

Optical imaging was performed at the Preclinical Imaging Technology Center at the Crump Institute for Molecular Imaging at UCLA. 100 µl of D-luciferin (GoldBio) dissolved in phosphate buffer saline without Ca2+ or Mg2+ (30 mg/ml) was introduced to each animal by intraperitoneal (IP) injection. After 7 minutes of conscious uptake, mice were anesthetized by inhalation of 2.6% isoflurane in oxygen and placed in dedicated imaging chambers. The IVIS Lumina 2 imaging system (Caliper Life Sciences) was utilized for *in vivo* bioluminescent imaging. Luminescence was measured over 3 minutes, and a corresponding photograph of the mice was taken and co-registered with the luminescent image for signal localization. Images were analyzed by drawing regions of interest and quantified as total flux (photons/second) with the Living Image software package (Perkin Elmer).

Western Blot and Immunohistochemistry

Western blots were performed using the following antibodies: mouse anti CPT1A (abcam, 128568), rabbit anti CPT1C (LsBio, LS-C167010), rabbit and mouse anti beta-actin (Abcam). To prepare samples for immunohistochemical analysis, Mouse brains from U87 transplant experiments were perfused using 4% paraformaldehyde (PFA) and incubated overnight in PFA at 4°C for 24 hours. Tissue was washed with PBS and incubated in 20% sucrose at 4°C for a

minimum of 24 hours in preparation for sectioning on a cryostat. Sections (20 μm thick) were post-fixed for 15 minutes with cold 4% paraformaldehyde followed by 3 washes with TBS prior to performing immunohistochemistry for CPT1A.

Acute etomoxir treatment and fatty acid and ketone supplementation

Dissociated cultures were plated at a density of $5x10^4$ cells/ml in triplicate in gliomasphere defined media containing 25 mM glucose unless otherwise indicated. Cells were incubated for 24 hours after which point 100 μM etomoxir (ETOM) ((+)-Etomoxir sodium salt hydrate, Sigma Aldrich, #E1905) was added to each sample and again on day 4. For FA and ketone supplementation, $4x10^3$ cells were plated per well in 96-well plates and incubated for 24 hours, after which either FAs or ketones were added to yield the following final concentrations of each. For FA: 25-200 μM palmitate (Sigma Aldrich, #P0500) bound to fatty-acid free BSA (5g/50mL in 10% PBS) (Sigma Aldrich, #A1595) and 500 μM carnitine (Sigma Aldrich, # C0283). For 3-OHB (Sigma Aldrich, #166898) final concentrations were 1.25-10 mM. Blood plasma concentrations of these substrates in healthy adults range from 111-260 μM palmitate and 67 μM carnitine (Borch et al., 2012; Cunnane et al., 2012; Jensen et al., 1989). Cells were allowed to grow for the indicated period of time prior to analysis using the Dojindo Cell Counting Kit 8 (#CK04-20) according to manufacturer instructions.

Cell growth analysis

Single-cell suspensions were made from bulk cultures of the U87 and patient-derived glioma cell lines and counted using a Countess automated cell counter. Cells were plated at $5x10^4$ cells/mL in 6-well plates and grown as gliomaspheres in control or experimental conditions. For

ETOM experiments, cells were treated 24 hours after initial plating and treatment was re-administered on Day 4. After 7 days the gliomaspheres in each well were fully dissociated and re-counted to assess changes in cell number during treatment. This analysis of cell number examines both cell survival and proliferation in response to treatment.

Proliferation analysis with bromodeoxyuridine (BrdU)

Single cell suspensions were plated as a monolayer on laminin-coated glass coverslips (Sigma, L2020) in 24-well plates followed by a 4 day ETOM treatment. Two BrdU pulses were given 2 hours apart and cells were fixed for 15 minutes with 4% paraformaldehyde. Coverslips were washed with PBS and immunocytochemistry was performed to assess the percentage of BrdU-positive cells by visual microscopic cell counts.

Annexin V/PI Flow Cytometry Analysis

Single cell samples were treated with 100 μM ETOM for 4 days after which spheres were re-dissociated with 200 μl accumax, centrifuged, and washed with PBS. Annexin V/propidium iodide (PI) staining was carried out according to manufacturer protocol using the Annexin V APC flow cytometry kit (Thermo Fisher) while including a 1 μl/ml final concentration of PI. Samples were gently mixed and incubated with Annexin V/PI binding buffer and incubated for 15 minutes at room temperature protected from light. Samples were kept on ice and analyzed within 1 hour by flow cytometry.

LC-MS with fully labeled ^{13}C palmitate

Gliomaspheres were dissociated into single cells with Accumax™ and $2x10^5$ cells were cultured for 48 hours in 2.5 mM glucose media in triplicate for each sample. Cells were then rinsed with PBS and re-plated in 2.5 mM glucose media, either unlabeled or containing 200 μM fully-labeled ^{13}C-palmitic acid for an additional 48 hours. Cells were then centrifuged and rinsed with 1ml ice-cold 150 mM ammonium acetate (pH 7.3). Centrifugation was performed again and 1ml of ice-cold 80% methanol was added. Cells were transferred to an Eppendorf tube, and 10 nmol norvaline (Sigma-Aldrich, N7502) was added to each sample. Samples were centrifuged for 5 min at top speed and the supernatant was transferred into a glass vial. Samples were resuspended in 200 μL cold 80% methanol, followed again by centrifugation, after which the supernatant was added to the glass vial. Samples were dried in an EZ-2Elite evaporator. The remaining pellet was resuspended in RIPA buffer and a Bradford assay was performed to quantify total protein concentration for sample normalization. Dried metabolites were resuspended in 50% ACN and 5 μL loaded onto a Luna 3 μm NH2 100 A (150 × 2.0 mm) column (Phenomenex). The chromatographic separation was performed on an UltiMate 3000 RSLC (Thermo Scientific) with mobile phases A (5 mM NH4AcO pH 9.9) and B (ACN) and a flow rate of 200 μL/min. The gradient from 15% A to 95% A over 18 min was followed by 9 min isocratic flow at 95% A and re-equilibration. Metabolite detection was achieved with a Thermo Scientific Q Exactive mass spectrometer run in polarity switching mode (+3.5 kV/− 3.5 kV). TraceFinder 4.1 (Thermo Scientific) was used to quantify the area under the curve for metabolites by using accurate mass measurements (< 3 ppm) and the retention time of purchased reference standards. Relative amounts of metabolites were calculated by summing up all isotopologues of a given metabolite and normalized to cell number. Correction for naturally occurring ^{13}C as well as calculation of fractional contributions and clustering analyses were done in R. Fractional contribution was

calculated as $\sum_{i=1}^{n} \frac{M_i \cdot i}{n}$, where n is the number of carbons in the metabolite, i is the iteration of each possible ^{13}C-labeled carbon, and M_i is the relative abundance of the i^{th} isotopologue. The relative amount is calculated as the sum of all isotopologues of each metabolite normalized to total protein.

Statistical Analysis

Statistical analysis was performed using either Microsoft Excel, GraphPad Prism, or IBM SPSS software with guidance from the UCLA Institute for Digital Research & Education. For tumor growth, flux data was lognormalized and statistical significance was determined using a mixed effects model with repeated measures for individual animals and Tukey's post-hoc pairwise analyses. Survival was analyzed by Kaplan-Meier curves with pairwise Mantel-Cox post-hoc analyses. For other comparative samples, normality of distributions was determined by Shapiro tests and significance was determined using either ANOVA or a univariate generalized linear model model and two-tailed Student's T-tests where appropriate. All quantitative data and associated error bars represent the mean ± either the standard deviation (SD) or standard error of the mean (SEM) as indicated for each figure. Experiments were performed in triplicate at a minimum, with 95% confidence intervals and p values calculated for relevant comparison. For all figures, p values are represented as follows: NS = not signifant, * = $p<0.05$, ** = $p<0.01$, *** = $p<0.001$.